



Published in final edited form as:

Neuroimage. 2013 September ; 78: 111–134. doi:10.1016/j.neuroimage.2013.04.018.

SURFACE FLUID REGISTRATION OF CONFORMAL REPRESENTATION: APPLICATION TO DETECT DISEASE BURDEN AND GENETIC INFLUENCE ON HIPPOCAMPUS

Jie Shi, MS¹, Paul M. Thompson, PhD², Boris Gutman, BS², Yalin Wang, PhD¹, and the Alzheimer's Disease Neuroimaging Initiative*

¹School of Computing, Informatics, and Decision Systems Engineering, Arizona State University, Tempe, AZ, USA

²Laboratory of Neuro Imaging, UCLA Dept. of Neurology, UCLA School of Medicine, Los Angeles, CA, USA

Abstract

In this paper, we develop a new automated surface registration system based on surface conformal parameterization by holomorphic 1-forms, inverse consistent surface fluid registration, and multivariate tensor-based morphometry (mTBM). First, we conformally map a surface onto a planar rectangle space with holomorphic 1-forms. Second, we compute surface conformal representation by combining its local conformal factor and mean curvature and linearly scale the dynamic range of the conformal representation to form the feature image of the surface. Third, we align the feature image with a chosen template image via the fluid image registration algorithm, which has been extended into the curvilinear coordinates to adjust for the distortion introduced by surface parameterization. The inverse consistent image registration algorithm is also incorporated in the system to jointly estimate the forward and inverse transformations between the study and template images. This alignment induces a corresponding deformation on the surface. We tested the system on Alzheimer's Disease Neuroimaging Initiative (ADNI) baseline dataset to study AD symptoms on hippocampus. In our system, by modeling a hippocampus as a 3D parametric surface, we nonlinearly registered each surface with a selected template surface. Then we used mTBM to analyze the morphometry difference between diagnostic groups. Experimental results show that the new system has better performance than two publically available subcortical surface registration tools: FIRST and SPHARM. We also analyzed the genetic influence of the Apolipoprotein E ϵ 4 allele (ApoE4), which is considered as the most prevalent risk factor for AD. Our work successfully detected statistically significant difference between ApoE4 carriers and non-carriers in both patients of mild cognitive impairment (MCI) and healthy control subjects. The

© 2013 Elsevier Inc. All rights reserved.

Please address correspondence to: Dr. Yalin Wang School of Computing, Informatics, and Decision Systems Engineering Arizona State University P.O. Box 878809 Tempe, AZ 85287 USA **Phone:** (480) 965-6871 **Fax:** (480) 965-2751 ylwang@asu.edu.

***Acknowledgments and Author Contributions:** Data used in preparation of this article were obtained from the Alzheimer's Disease Neuroimaging Initiative (ADNI) database (adni.loni.ucla.edu). As such, the investigators within the ADNI contributed to the design and implementation of ADNI and/or provided data but did not participate in analysis or writing of this report. A complete listing of ADNI investigators can be found at: http://adni.loni.ucla.edu/wp-content/uploads/how_to_apply/ADNI_Acknowledgement_List.pdf. Additional support was provided by the National Institute on Aging (AG016570 to PMT), the National Library of Medicine, the National Institute for Biomedical Imaging and Bioengineering, and the National Center for Research Resources (LM05639, EB01651, RR019771 to PMT).

Publisher's Disclaimer: This is a PDF file of an unedited manuscript that has been accepted for publication. As a service to our customers we are providing this early version of the manuscript. The manuscript will undergo copyediting, typesetting, and review of the resulting proof before it is published in its final citable form. Please note that during the production process errors may be discovered which could affect the content, and all legal disclaimers that apply to the journal pertain.

results show evidence that the ApoE genotype may be associated with accelerated brain atrophy so that our work provides a new MRI analysis tool that may help presymptomatic AD research.

Keywords

nonlinear image registration; surface conformal parameterization; conformal representation; surface fluid registration; tensor-based morphometry; presymptomatic AD

1. INTRODUCTION

Most brain MRI scanning protocols have been designed to acquire volumetric data on the anatomy of a subject. Various non-linear brain volume-based registration methods (Christensen et al., 1996; Shen and Davatzikos, 2002; Yanovsky et al., 2009) have been developed for brain volume image analysis. However, when registering structural MR images, the volume-based methods have much more difficulty with the highly convoluted cortical surfaces due to the complexity and variability of the sulci and gyri. Early research (Thompson and Toga, 1996; Fischl et al., 1999; Van Essen et al., 2001; Thompson et al., 2004b) has demonstrated that surface-based brain mapping may offer advantages over volume-based brain mapping as a method to study the structural features of the brain, such as cortical gray matter thickness, as well as the complexity and change patterns in the brain due to disease or developmental processes. To register brain surfaces, a common approach is to compute dense correspondence vector fields that match one surface with another. Often, higher order correspondences must be enforced between specific anatomical points, curved landmarks, or subregions lying within two surfaces. This is often achieved by first mapping each of the 3D surfaces to a canonical parameter space such as a sphere (Bakircioglu et al., 1999; Fischl et al., 1999; Yeo et al., 2010) or a planar domain (Thompson and Toga, 2002; Thompson et al., 2004b; Leow et al., 2005b). A flow, computed in the parameter space of the two surfaces, induces a correspondence field in 3D (Davatzikos, 1996; Thompson et al., 2000). This flow can be constrained using anatomic landmark points or curves (Pantazis et al., 2010; Zhong and Qiu, 2010; Auzias et al., 2011), by subregions of interest (Qiu and Miller, 2008), by constraining the mapping of surface regions represented implicitly using level sets (Leow et al., 2005b), or by using currents to represent anatomical variation (Vaillant and Glaunes, 2005; Vaillant et al., 2007; Durrleman et al., 2008). Feature correspondence between two surfaces can be optimized by using the ℓ_2 -norm to measure differences in curvature profiles or convexity (Fischl et al., 1999) or by using mutual information to align scalar fields of various differential geometric parameters defined on the surface (Wang et al., 2005b). Artificial neural networks may also be used to rule out or favor certain types of feature matches (Pitiot et al., 2003). Finally, correspondences may be determined by using a minimum description length (MDL) principle, based on the compactness of the covariance of the resulting shape model (Davies et al., 2002; Thodberg, 2003). A key direction in surface registration research has been the computation of a diffeomorphic surface map that matches automatically identified surface features.

MRI-based measures of atrophy in several structural measures, including whole-brain (Fox et al., 1999; Chen et al., 2007; Stonnington et al., 2010), entorhinal cortex (Cardenas et al., 2011), hippocampus (Jack et al., 2003; Thompson et al., 2004a; Wang et al., 2006; den Heijer et al., 2010; Wolz et al., 2010), and temporal lobe volumes (Hua et al., 2011), as well as ventricular enlargement (Jack et al., 2003; Thompson et al., 2004a), correlate closely with changes in cognitive performance, supporting their validity as markers of disease progression (Apostolova et al., 2010b; Costafreda et al., 2011). Of all the MRI markers of Alzheimer's disease (AD), hippocampal atrophy assessed on high-resolution T1-weighted MRI is the best established and validated. One of the key research topics for clinical

assessment in diagnosis and monitoring of progression of patients with suspected Alzheimer dementia is to establish and validate efficient biomarkers based on subcortical structures including hippocampus. Although most subcortical structure analysis work used volume as the atrophy measurement (Jack et al., 2003; Jack et al., 2004; Ridha et al., 2008; Holland et al., 2009; den Heijer et al., 2010; Dewey et al., 2010; Wolz et al., 2010), recent researches (Thompson et al., 2004a; Styner et al., 2005; Wang et al., 2006; Ferrarini et al., 2008; Chou et al., 2009; Morra et al., 2009b; Apostolova et al., 2010b; Apostolova et al., 2010c; Madsen et al., 2010; Qiu et al., 2010; Costafreda et al., 2011) have demonstrated that surface-based subcortical structure analysis may offer advantages over volume measure. For example, the surface-based methods have studied patterns of hippocampal subfield atrophy and detailed point-wise correlation between atrophy and cognitive functions/biological markers. There are several methods that match surfaces of subcortical structures using parametric surfaces, such as contour parameterization (Thompson et al., 2004a; Morra et al., 2009a; Chou et al., 2010), SPHARM (spherical harmonic) methods (Styner et al., 2005), large deformation diffeomorphism metric matching (LDDMM) (Qiu et al., 2008; Qiu et al., 2009a; Qiu et al., 2010), Laplacian-Beltrami eigen-features (Shi et al., 2009), multi-resolution geodesic construction on Riemannian manifolds (Cho et al., 2011) and Beltrami holomorphic flow (Lui et al., 2010). Recently, we introduced a set of parametric surfaces using concepts from conformal geometry which provided a rigorous framework for representing, splitting, parameterizing, matching and measuring subcortical surfaces (Wang et al., 2010b). It has been successfully applied to study HIV/AIDS (Wang et al., 2010b) and AD (Wang et al., 2011b). Even so, an automated substructure surface registration system that uses complete surface geometric features for a diffeomorphic mapping is still highly advantageous.

Using holomorphic 1-forms, a global conformal parameterization can be developed to map a surface to a rectangular domain in the Euclidean plane (Wang et al., 2009a). On the other hand, fluid registration has been widely used to drive a large-deformation diffeomorphic flow for image correspondence. By adjusting the viscous fluid method to parametrically match scalar-valued signals representing surface geometry, we derive a method for landmark-free surface registration. Since both kinds of mappings are diffeomorphic, their composition leads to diffeomorphic shape correspondence (i.e., a smooth, one-to-one correspondence). Wang et al. (2005b) proposed an automated surface fluid registration method based on conformal mapping and image fluid registration, and applied it to register human faces and human hippocampal surfaces. Here, we extend the Navier-Stokes equation in Wang et al. (2005a; 2005b) into general surface space using covariant derivatives. Due to the simple Riemannian metric induced by conformal parameterization, the general Navier-Stokes equation can be easily adjusted for area distortion. As pointed out in Leow et al. (2005a), inverse consistent registration method is more robust than the traditional unidirectional registration. Leow et al. (2005a) presented a novel inverse consistent image registration scheme with linear elastic regularization. Chiang et al. (2008) extended the method in Leow et al. (2005a) with viscous fluid regularization to enable large deformations, and applied the method to diffusion tensor images. We extend the method proposed in Chiang et al. (2008) to surfaces. Solving the Navier-Stokes equation on the surface and matching geometrically-informed scalar functions, we develop an inverse-consistent surface registration algorithm. In this paper we apply our algorithm to hippocampal shapes in the ADNI dataset.

In general, in order to study structural features of the brain, such as cortical gray matter thickness, complexity, and deformation over time, etc., there are roughly two different approaches, deformation-based morphometry (DBM) (Ashburner et al., 1998; Chung et al., 2001; Chung et al., 2003; Wang et al., 2003) and tensor-based morphometry (TBM) (Davatzikos et al., 1996; Thompson et al., 2000; Chung et al., 2008). DBM tends to analyze 3D displacement vector fields encoding relative positional differences across subjects, while TBM tends to examine spatial derivatives of the deformation maps registering brains to a

common template, constructing morphological tensor maps such as the Jacobian determinant, torsion or vorticity. One advantage of TBM for surface morphometry is that TBM can make use of the intrinsic Riemannian surface metric to characterize local anatomical changes. Chung et al. (2008) showed that the single value of the determinant of Jacobian can reliably detect surface morphometry due to autism. In our system, we use multivariate statistics based on surface deformation tensors to study brain surface morphometry as proposed in (Leporé et al., 2008; Wang et al., 2008). The multivariate tensor-based morphometry (mTBM) computes statistics from the Riemannian metric tensors that retain the full information in the deformation tensor fields, thus may be more powerful in detecting surface difference than many other statistics (Wang et al., 2009a; Wang et al., 2010b; Wang et al., 2011b; Wang et al., 2012b). Our hypothesis is that, together with mTBM as the surface statistics, our surface fluid registration method may help boost statistical power to detect disease burden and genetic influence on hippocampal morphometry compared with some existing researches in the literature. Here we set out to validate our algorithm in the Alzheimer's Disease Neuroimaging Initiative (ADNI) baseline dataset.

Fig. 1 summarizes the overall step sequence in our system. The brain MR image data was from ADNI baseline dataset. The hippocampal regions and surfaces were segmented and constructed automatically. We then computed hippocampal surface conformal parameterization with holomorphic 1-forms and obtained their feature images consisting of conformal factor and mean curvature. With the inverse consistent surface fluid registration method, we enforced symmetric displacements in both surfaces ($\mathbf{h}(\mathbf{x})$ denotes the forward mapping and $\mathbf{g}(\mathbf{x})$ denotes the inverse mapping, where $\mathbf{g}(\mathbf{x}) = \mathbf{h}^{-1}(\mathbf{x})$). Multivariate statistics were computed to study differences between diagnostically different groups and the genetic influence on Alzheimer's disease.

2. SUBJECTS AND METHODS

2.1. Subjects

Data used in the preparation of this article were obtained from the Alzheimer's Disease Neuroimaging Initiative (ADNI) database (adni.loni.ucla.edu). The ADNI was launched in 2003 by the National Institute on Aging (NIA), the National Institute of Biomedical Imaging and Bioengineering (NIBIB), the Food and Drug Administration (FDA), private pharmaceutical companies and non-profit organizations, as a \$60 million, 5-year public-private partnership. The primary goal of ADNI has been to test whether serial magnetic resonance imaging (MRI), positron emission tomography (PET), other biological markers, and clinical and neuropsychological assessment can be combined to measure the progression of mild cognitive impairment (MCI) and early Alzheimer's disease (AD). Determination of sensitive and specific markers of very early AD progression is intended to aid researchers and clinicians to develop new treatments and monitor their effectiveness, as well as lessen the time and cost of clinical trials.

The Principal Investigator of this initiative is Michael W. Weiner, MD, VA Medical Center and University of California – San Francisco. ADNI is the result of efforts of many co-investigators from a broad range of academic institutions and private corporations, and subjects have been recruited from over 50 sites across the U.S. and Canada. The initial goal of ADNI was to recruit 800 adults, ages 55 to 90, to participate in the research, approximately 200 cognitively normal older individuals to be followed for 3 years, 400 people with MCI to be followed for 3 years and 200 people with early AD to be followed for 2 years. For up-to-date information, see www.adni-info.org.

At the time of downloading (09/2010), the baseline dataset consisted of 843 adults, ages 55 to 90, including 233 elderly healthy controls, 410 subjects with mild cognitive impairment (MCI) and 200 AD patients. In this study, we manually excluded 1 subject from the control group and 2 subjects from the MCI group because of name duplication. For subjects with duplicated names, we retained the one which was the repeated scan. All subjects underwent thorough clinical and cognitive assessment at the time of acquisition, including the Mini-Mental State Examination (MMSE) score (Folstein et al., 1975), Clinical Dementia Rating (CDR)(Berg, 1988), and Delayed Logical Memory Test(Wechsler, 1987).

2.2. Image Acquisition and Preprocessing

All T1-weighted images were automatically segmented using FIRST (<http://www.fmrib.ox.ac.uk/fsl/fsl/list.html>). FIRST is an integrated surface registration and segmentation tool developed as part of the FSL library, which is written mainly by members of the Analysis Group, FMRIB, Oxford, UK. FIRST is able to extract subcortical structures and assign the image voxels with different numerical labels. Then the binary image segmentation can be obtained by a simple threshold process. After obtaining the binary segmentation, we used a topology-preserving level set method (Han et al., 2003) to build surface models. Based on that, the marching cubes algorithm (Lorensen and Cline, 1987) was applied to obtain triangular surface meshes. However, the surface models constructed from medical image data, which has limited resolution and noise from scanning, may contain much noise. Surface smoothing may help restore the original shape and overcome partial volume effects. Furthermore, the triangular meshes obtained by the marching cubes algorithm (Lorensen and Cline, 1987) often contain obtuse angles, which make the meshes inappropriate for direct use in conformal parameterization. In our system, to compute the conformal parameterization, we need first compute harmonic forms and it requires solving a linear system to minimize harmonic energy (Wang et al., 2011b). In the finite element formulation, there is a cotangent weight term (Gu et al., 2004a) which should be positive. The system became unsolvable if there are too many obtuse angles (negative cotangent weight terms). Thus mesh smoothing is needed before any further processing. Many mesh smoothing algorithms have been proposed. In (Taubin, 1995), Taubin proposed a simple, linear and isotropic method to improve the smoothness of a surface mesh. This method is fast because it does not rely on expensive functional minimizations. Some variants of this algorithm have also been developed (Desbrun et al., 1999; Ohtake et al., 2000). However, these techniques are isotropic, thus indiscriminately smooth noise and salient surface features. Recently, feature-preserving mesh smoothing methods (Clarenz et al., 2000; Desbrun et al., 2000; Zhang and Fiume, 2002; Bajaj and Xu, 2003; Fleishman et al., 2003; Jones et al., 2003; Meyer et al., 2003; Sun et al., 2007; Sun et al., 2008; Li et al., 2009) have also drawn more and more interests. In this paper, we applied a two-step mesh smoothing method to all the surfaces. The smoothing process consists of mesh simplification using “progressive meshes” (Hoppe, 1996) and mesh refinement by Loop subdivision surface (Loop, 1987). All the meshes were smoothed by 5 iterations of mesh simplification using “progressive meshes” and Loop subdivision. In order to smooth the surfaces while preserve surface features, we gradually increased the face numbers of the surfaces in each iteration. As a result, we obtained relatively smooth but accurate surfaces that are suitable for computing derivative maps. **Fig. 2** illustrates the histograms of the Hausdorff distances between the smoothed meshes and the original meshes for both the left and right hippocampi. We can see from the figure that the majority of the absolute distances fall into the range [0.9, 1.1] with the unit as millimeter. Given the volumes of hippocampus lie between 3000 and 4000 mm³ (Hasboun et al., 1996; Hickie et al., 2005; Ystad et al., 2009; Carmichael, 2011), our smoothed meshes can be regarded as accurate approximations of the original surfaces. We applied this method in our prior subcortical surface analysis work (Wang et al., 2010b; Wang et al., 2011b). From our experience, a continuous subdivision

and mesh simplification process will generally eliminate the obtuse angles and improve the mesh quality. Later all the smoothed meshes were normalized into a standard space using affine transformation with a 9-parameter (3 parameters for translation, 3 parameters for rotation, and 3 parameters for scaling) matrix that was computed by FIRST. In our study, 1 subject from each group (AD, MCI, and control) failed the FIRST segmentation step probably due to the original images' resolution or contrast issues. We also manually checked all the constructed and smoothed meshes and excluded 5 AD, 5 MCI, and 3 control subjects due to wrong topologies. As a result, the baseline MR hippocampus image data of 194 AD (age: 76.1 ± 7.6 years), 402 MCI (age: 75.0 ± 7.3 years), and 228 controls (age: 76.0 ± 5.0 years) were studied using the new system within the scope of this paper.

2.3. Surface Conformal Parameterization with Holomorphic 1-Forms

Let S be a surface in \mathbb{R}^3 with an atlas $\{(U_\alpha, z_\alpha)\}$, where (U_α, z_α) is a coordinate chart defined on S . The atlas thus is a set of consistent charts with smooth transition functions between overlapping charts. Here $z_\alpha: U_\alpha \rightarrow \mathbb{C}$ maps an open set $U_\alpha \subset S$ to a complex plane \mathbb{C} . If on any chart (U_α, z_α) in the atlas, the Riemannian metric or the first fundamental form can be formulated as $ds^2 = \lambda(z_\alpha)^2 dz_\alpha d\bar{z}_\alpha$, and the transition maps

$z_\beta \circ z_\alpha^{-1}: z_\alpha(U_\alpha \cap U_\beta) \rightarrow z_\beta(U_\alpha \cap U_\beta)$ are holomorphic, the atlas could be called conformal. Given a conformal atlas, a chart is compatible with the atlas if adding this chart still generates a conformal atlas. A conformal structure is obtained by adding all possible compatible charts to a conformal atlas. A Riemann surface is a surface with a conformal structure. All metric oriented surfaces are Riemann surfaces. One coordinate chart in the conformal structure introduces a *conformal parameterization* between a surface patch and the image plane. The conformal parameterization is angle-preserving and intrinsic to the surface geometry (Do Carmo, 1976; Guggenheimer, 1977).

For a Riemann surface S with genus $g > 0$, its conformal structure can always be represented in terms of a holomorphic 1-form basis, which is a set of $2g$ functions $\tau_i: K_1 \rightarrow \mathbb{C}$, $i = 1, \dots, 2g$ (Wang et al., 2007). Here, K_1 represents the simplicial 1-complex*. Any holomorphic 1-form τ is a linear combination of these functions. This finite-dimensional linear space generates all possible conformal parameterizations of surface S and the quality of a global conformal parameterization is fundamentally determined by the choice of the holomorphic 1-form (Wang et al., 2007; Wang et al., 2011b). **By considering the holomorphic 1-form as an \mathbb{R}^2 function, the conformal parameterization $\phi: S \rightarrow \mathbb{R}^2$ at point p can be computed by integrating the holomorphic 1-form:**

$$\phi(p) = \int_{\gamma} \tau. \quad (1)$$

where γ is an arbitrary path joining p to a fixed point p_0 on the surface. The details of our holomorphic 1-form based conformal parameterization algorithms were reported in our prior work (Wang et al., 2007; Wang et al., 2011b). **Fig.3** (a) illustrates a pair of hippocampal surfaces and their conformal parameterizations to a rectangular domain.

2.4. Surface Conformal Representation

It has been known that surface registration requires defining a lot of landmarks in order to align corresponding functional regions. Labeling features could be accurate but time-

*In mathematics, a simplicial complex is a topological space that is constructed by gluing together points, line segments, triangles, and their n -dimensional counterparts. A simplicial k -complex K_k is a simplicial complex where the largest dimension of any component in K_k equals to k . In our settings, a simplicial 1-complex is an edge.

consuming. Here we show that surface conformal parameterization could represent surface geometric features, thus avoiding the manual definition of landmarks.

For a general surface and its conformal parameterization $\phi: S \rightarrow \mathbb{R}^2$, the conformal factor at a point p can be determined by the formula:

$$\lambda(p) = \frac{\text{Area}(B_\epsilon(p))}{\text{Area}(\phi(B_\epsilon(p)))}. \quad (2)$$

where $B_\epsilon(p)$ is an open ball around with a radius ϵ . The conformal factor λ encodes a lot of geometric information about the surface and can be used to compute curvatures and geodesic. In our system, we compute the surface mean curvatures only from the derivatives of the conformal factors as proposed in Lui et al. (2008a), instead of the three coordinate functions and the normal, which are generally more sensitive to digitization errors. Mathematically, the mean curvature is defined as:

$$H = \frac{1}{2\lambda} \text{sign}(\phi) |\Delta\phi| \quad (3)$$

where $\text{sign}(\phi) = \frac{\langle \Delta\phi, \vec{N} \rangle}{|\Delta\phi|}$. Using this formulation of H , we need to use the surface normal \vec{N} only when computing $\text{sign}(\phi)$, which takes the value 1 or -1. Thus, the surface normal does not need to be accurately estimated and still we can get more accurate mean curvatures. Using the Gauss and Codazzi equations, one can prove that the conformal factor and mean curvature uniquely determine a closed surface in \mathbb{R}^3 , up to a rigid motion (Gu et al., 2004b). We call them the *conformal representation* of the surface. **Fig.3** (b) shows the computed conformal factor (left) and mean curvature (right) on a hippocampal surface with color indices according to the values. Since conformal factor and mean curvature encode both surface intrinsic structure and 3D embedding information, they are complete surface features to be used for solving surface registration problems (Gu and Vemuri, 2004; Wang et al., 2005a).

2.5. Inverse Consistent Surface Fluid Registration

After computing surface geometric features, we align surfaces in the parameter domain with a fluid registration technique to maintain smooth, one-to-one topology (Christensen et al., 1996). Using conformal mapping, we essentially convert the surface registration problem to an image registration problem. In our prior work (Wang et al., 2005a), we proposed an automated surface fluid registration method combining conformal mapping and image fluid registration (D'Agostino et al., 2003) with mutual information (Kim et al., 1997; Meyer et al., 1997; West et al., 1997; Rueckert et al., 1999; Hermosillo, 2002) as the driving force of the viscous fluid. In Wang et al. (2005a), the mutual information between two surface feature images, i.e., the conformal representations of the two surfaces that need to be registered, was maximized by the viscous fluid flow as in D'Agostino et al. (2003). On \mathbb{R}^2 , fluid flow is governed by the Navier-Stokes equation. For compressible fluid flow, we have

$$\mu \Delta \mathbf{v}(\mathbf{x}) + (\mu + \tau) \nabla (\nabla \cdot \mathbf{v}(\mathbf{x})) = \mathbf{f}(\mathbf{x}, \mathbf{u}(\mathbf{x})). \quad (4)$$

Here $\mathbf{v}(\mathbf{x})$ is the deformation velocity, μ and τ are the viscosity constants. $\mathbf{f}(\mathbf{x}, \mathbf{u}(\mathbf{x}))$ is the force field that is used to drive the fluid flow, which was defined as the mutual information in Wang et al. (2005a).

To simulate fluid flow on Riemann surfaces, we need to extend **Eq. 4** into surface space by the manifold version of Laplacian and divergence (Aris, 1989; Stam, 2003; Lui et al., 2005). By covariant derivatives, the Navier-Stokes equation for Riemann surface can be defined as:

$$\frac{\mu}{\lambda} \Delta v + \frac{\mu + \tau}{\lambda} \nabla (\nabla \cdot v) = f. \quad (5)$$

where λ is the conformal factor as introduced in Sec. 2.4. Please refer the appendix A for the derivation of **Eq. 5**. It is well known that area distortion is an inevitable problem of conformal parameterization. However, considering the definition of conformal factor λ as **Eq. 2**, we can see that conformal factor is a smooth function which describes the stretching effect of conformal parameterization (Lui et al., 2008b). In **Eq. 5**, by factoring out the conformal factor λ , the flow induced in the parameter domain is adjusted for the area distortion introduced by the conformal parameterization. As a result, **Eq. 5** is now governing fluid flow on the manifolds. In this paper, considering that hippocampi across the population should have similar shapes, we assume the conformal representations of different hippocampi have similar intensity range and distribution. Thus, the body force f in **Eq. 5** driving the fluid flow in this paper is defined as the sum of squared intensity differences (SSD) between the deforming image and the template image. In our experiments, the SSD based energy formulation has similar performance with mutual information energy which was adopted in our prior work (Wang et al., 2005a) while significantly improves algorithm efficiency compared with the latter method. As shown in **Fig. 4**, we illustrate the performance of the inverse consistent fluid registration driven by SSD and mutual information respectively, on the synthetic C-shape images. As can be seen from the figures, these two types of driving forces were able to obtain similar registration results while the time cost by SSD was 14.15 seconds. It was much more efficient than mutual information based energy formulation, which ran up to 1730.15 seconds. Both algorithms were executed on a 2.66GHz Intel Quad CPU Q8400 PC with Windows 7 64-bit operating system. Given the large number of surfaces to be registered, we chose to adopt SSD based energy formulation for improved efficiency (Christensen, 1994; Bro-Nielsen and Gramkow, 1996). Since conformal mapping and fluid registration generate diffeomorphic mappings, a diffeomorphic surface-to-surface mapping is then recovered that matches surfaces in 3D.

As pointed out in Leow et al. (2005a), image registration problem should be symmetric, i.e., the correspondences established between the two images should not depend on the order we use to compare them. However, traditional non-linear image registration algorithms are not symmetric, thus the deformation field depends on which image is assigned as the deforming image and which image the non-deforming target image. Furthermore, the asymmetric algorithms tend to penalize the expansion of image regions more than the shrinkage (Rey et al., 2002), making these methods problematic in applications where the Jacobian of the mappings is interpreted as measuring anatomical tissue loss or expansion. Many inverse consistent registration algorithms (Christensen and Johnson, 2001; Shi et al., 2009; Reuter et al., 2010; Reuter and Fischl, 2011) have been proposed to overcome the shortcomings of conventional inverse non-consistent methods. Leow et al. (2005a) proposed a novel inverse consistent image registration method. Instead of enforcing inverse consistency using an additional penalty that penalizes inconsistency error as in Christensen and Johnson (2001), the method in Leow et al. (2005a) directly modeled the reverse mapping by inverting the forward mapping. Chiang et al. (2008) replaced the linear elastic regularizer in Leow et al. (2005a) with the fluid regularization to enable large deformations and applied the inverse consistent fluid registration algorithm to diffusion tensor images. Here with the inverse consistent scheme proposed in Chiang et al. (2008), we extend **Eq. 5** into an inverse consistent surface fluid registration method.

Let $I_1(x)$, $I_2(x)$ be two images, using the sum of squared intensity differences as the matching cost function, the inverse consistent image registration problem seeks two mappings $\mathbf{h}(x)$ and $\mathbf{g}(x)$ to minimize the following energy function:

$$E(I_1(x), I_2(x)) = \int_{\Omega} |I_1(\mathbf{h}(x)) - I_2(x)|^2 dx + \alpha R(\mathbf{h}(x)) + \int_{\Omega} |I_2(\mathbf{g}(x)) - I_1(x)|^2 dx + \alpha R(\mathbf{g}(x)) \quad (6)$$

where $\mathbf{h}(x) = x - \mathbf{u}_f(x)$ is the mapping from image I_1 to image I_2 (forward direction) and $\mathbf{u}_f(x)$ is the forward displacement field. $\mathbf{g}(x) = x - \mathbf{u}_b(x)$ is the mapping from image I_2 to image I_1 (backward direction) and $\mathbf{u}_b(x)$ is the backward displacement field, $\mathbf{g}(x) = \mathbf{h}^{-1}(x)$. α is a positive scalar weighting of the regularization terms applied to the forward and backward mappings. Following prior work in fluid registration (Leow et al., 2005a; Chiang et al., 2008), we let $\alpha = 1$ to achieve a fast and stable convergence. **Eq. 6** is symmetric and does not depend on the order of I_1 and I_2 , i.e., $E(I_1, I_2) = E(I_2, I_1)$. **Suppose we have two surfaces S_1, S_2 and their conformal representation I_1, I_2 in \mathbb{R}^2 .** With fluid regularization scheme, $R(\mathbf{h}(x))$ is defined as $\int_0^1 \int_{\Omega} \|L v_f(x)\|^2 dx dt$ and $R(\mathbf{g}(x))$ is defined as $\int_0^1 \int_{\Omega} \|L v_b(x)\|^2 dx dt$ with the forward and backward velocities $v_f(x)$ and $v_b(x)$, respectively. $L = \frac{\mu}{\lambda} \Delta + \frac{\mu + \tau}{\lambda} \nabla(\nabla \cdot)$ is the surface linear operator as in **Eq. 5**. Then the energy function in **Eq. 6** can be minimized by solving for the velocities $v_f(x)$ and $v_b(x)$ in the following general Navier-Stokes equations:

$$\frac{\mu}{\lambda_{f,b}} \Delta v_{f,b} + \frac{\mu + \tau}{\lambda_{f,b}} \nabla(\nabla \cdot v_{f,b}) = f_{f,b} \quad (7)$$

where the forward force field $f_f = -[I_1(x - \mathbf{u}_f(x)) - I_2(x)] \nabla I_1(x - \mathbf{u}_f(x))$ and backward force field $f_b = -[I_2(x - \mathbf{u}_b(x)) - I_1(x)] \nabla I_2(x - \mathbf{u}_b(x))$. λ_f is the conformal factor of surface S_1 and λ_b is the conformal factor of surface S_2 .

With the mappings $\mathbf{h}(x)$, $\mathbf{g}(x)$ initialized as the identical mapping at $t = 0$, the forward and backward mappings at time t are given by the following equations as in (Leow et al., 2005a):

$$\begin{aligned} \mathbf{h}_t(x) &= \mathbf{h}_{t-1}(x) + \epsilon \eta_1(x) + \epsilon \eta_2(x) \\ \mathbf{g}_t(x) &= \mathbf{g}_{t-1}(x) + \epsilon \xi_1(x) + \epsilon \xi_2(x) \end{aligned} \quad (8)$$

Here, ϵ is an infinitesimally small positive time step. $\eta_1, \eta_2, \xi_1, \xi_2$ are computed as (Chiang et al., 2008):

$$\begin{aligned} \eta_1(x) &= -(\nabla \mathbf{h}_{t-1}(x)) v_f^{t-1}(x), \eta_2(x) = v_b^{t-1}(\mathbf{h}_{t-1}(x)) \\ \xi_1(x) &= v_f^{t-1}(\mathbf{g}_{t-1}(x)), \xi_2(x) = -(\nabla \mathbf{g}_{t-1}(x)) v_b^{t-1}(x) \end{aligned} \quad (9)$$

2.6. Multivariate Tensor-Based Morphometry Statistics

Suppose $\phi: S_1 \rightarrow S_2$ is a map from the surface S_1 to the surface S_2 . To simplify the formulation, we use the isothermal coordinates of both surfaces as the arguments. Let (u_1, v_1) be the isothermal coordinates of S_1 and S_2 . The Riemannian metric of S_i is represented as $\mathbf{g}_i = e^{2\lambda_i} (du_1^2 + dv_1^2)$, $i = 1, 2$. In the local parameters, the map ϕ can be represented as $\phi(u_1, v_1) = (\phi_1(u_1, v_1), \phi_2(u_1, v_1))$. The derivative map of ϕ is the linear map between the tangent spaces, $d\phi: TM(p) \rightarrow TM(\phi(p))$, induced by the map ϕ . In the local parameter domain, the derivative map is the Jacobian of ϕ :

$$d\phi = \begin{bmatrix} \frac{\partial\phi_1}{\partial u_1} & \frac{\partial\phi_1}{\partial v_1} \\ \frac{\partial\phi_2}{\partial u_1} & \frac{\partial\phi_2}{\partial v_1} \end{bmatrix}$$

Let the position vector of S_1 be $r(u_1, v_1)$. Denote the tangent vector fields as $\frac{\partial}{\partial u_1} = \frac{\partial r}{\partial u_1}$, $\frac{\partial}{\partial v_1} = \frac{\partial r}{\partial v_1}$. Because (u_1, v_1) are isothermal coordinates, $\frac{\partial}{\partial u_1}$ and $\frac{\partial}{\partial v_1}$ only differ by a rotation of $\pi/2$. Therefore, we can construct an orthonormal frame on the tangent plane of S_1 as

$$\left\{ e^{-\lambda_1} \frac{\partial}{\partial u_1}, e^{-\lambda_1} \frac{\partial}{\partial v_1} \right\}.$$

Similarly, we can construct an orthonormal frame on S_2 for its isothermal coordinates. Since any two surfaces are locally conformal (Hsiung, 1997), we can have an orthonormal frame on S_2 as $\left\{ e^{-\lambda_2} \frac{\partial}{\partial u_1}, e^{-\lambda_2} \frac{\partial}{\partial v_1} \right\}$. The derivative map under the orthonormal frames is represented as

$$d\phi = e^{\lambda_2 - \lambda_1} \begin{bmatrix} \frac{\partial\phi_1}{\partial u_1} & \frac{\partial\phi_1}{\partial v_1} \\ \frac{\partial\phi_2}{\partial u_1} & \frac{\partial\phi_2}{\partial v_1} \end{bmatrix}$$

In practice, smooth surfaces are approximated by triangle meshes. In the triangle mesh surface, the derivative map $d\phi$ is approximated by the linear map from one face $[v_1, v_2, v_3]$ to another $[w_1, w_2, w_3]$. First, the surfaces $[v_1, v_2, v_3]$ and $[w_1, w_2, w_3]$ are isometrically embedded onto the plane \mathbb{R}^2 (i.e., $\lambda_1 = \lambda_2 = 0$ in the above equation), the planar coordinates of the vertices v_i, w_j are denoted by the same symbol v_i, w_j . Then the Jacobian matrix for the derivative map $d\phi$ can be explicitly computed as (Wang et al., 2009a)

$$J = d\phi = [w_3 - w_1, w_2 - w_1] [v_3 - v_1, v_2 - v_1]^{-1}. \quad (10)$$

The deformation tensor can be defined as $S = (J^T J)^{\frac{1}{2}}$ (Chung et al., 2001; Hua et al., 2011). Instead of analyzing shape change based on the eigenvalues of the deformation tensor, a new family of metrics, the ‘‘Log-Euclidean metrics’’ (Arsigny et al., 2006) is considered in the multivariate tensor-based morphometry (mTBM). In this framework, Riemannian computations can be converted into Euclidean ones once tensors have been transformed into their matrix logarithms (Arsigny et al., 2006). This conversion makes computations on tensors easier to perform, as they are chosen such that the transformed values form a vector space, and statistical parameters can then be computed easily using the standard formulae for Euclidean spaces (Leporé et al., 2008; Wang et al., 2008).

To compute group differences with mTBM, we then apply Hotelling’s T^2 test (Hotelling, 1931; Cao and Worsley, 1999; Thirion et al., 2000; Kim et al., 2012) on sets of values in the log-Euclidean space of the deformation tensors. Given two groups of $n \times 1$ -dimensional vectors, $S_i, i = 1, 2, \dots, p, T_j, j = 1, 2, \dots, q$, we use the Mahalanobis distance M to measure the group mean difference,

$$M = \frac{N_S N_T}{N_S + N_T} (\bar{S} - \bar{T})^T \Sigma^{-1} (\bar{S} - \bar{T}). \quad (11)$$

where N_S and N_T are the number of subjects in the two groups, \bar{S} and \bar{T} are the means of the two groups and Σ is the combined covariance matrix of the two groups (Leporé et al., 2008; Wang et al., 2010b; Wang et al., 2011b). In our study, S and T are the log-Euclidean

metrics, e.g. $S_i = \log \left[(J_i^T J_i)^{\frac{1}{2}} \right]$, $i = 1, 2, \dots, p$ and $T_j = \log \left[(J_j^T J_j)^{\frac{1}{2}} \right]$, $j = 1, 2, \dots, q$. Since the statistic M is a uni-variate, our analysis does not introduce any bias because of the increase of the variable number.

3. RESULTS

3.1 Synthetic Surface Registration with Inverse Consistent Surface Fluid Registration

In order to validate the effectiveness of the proposed method, we generated two synthetic surfaces as shown in **Fig. 5** (a) and (b). The two C shapes have different sizes and positions. This can also be seen from the corresponding feature images at the bottom of **Fig. 5** (a) and (b). The feature images were generated by summing up the local conformal factor and the mean curvature, expressed in the conformal parameterization domain. The black lines drawn on the surfaces are used to show equal distances on the surfaces and represent the differences in their shapes. With the inverse consistent fluid registration, in **Fig. 5**(c) and (d), we can see that the feature image of surface 1 was successfully registered to the feature image of surface 2 and the feature image of surface 2 was also registered to the feature image of surface 1. With the forward and backward mappings obtained in the parameter domain, we induced a forward deformation and a backward deformation in surface 1 and surface 2, respectively. As we can see from **Fig. 5** (c) and (d), without changing the shape of the surfaces, the features on them are well aligned to each other.

3.2 Hippocampal Surface Registration with Inverse Consistent Surface Fluid Registration

We have developed an automatic algorithm to identify two landmark curves at the front and back of the hippocampal surface, representing its anterior junction with the amygdala, and its posterior limit as it turns into the white matter of the fornix (the hole boundaries are shown as blue curves in **Fig. 3** (a)) (Wang et al., 2011b). They are biologically valid and consistent landmarks across subjects. Given the hippocampal tube-like shape, these landmark curves can be automatically detected by checking the extreme points by searching along the first principle direction of geometric moments of surface (Elad et al., 2004; Zhang and Lu, 2004; Wang et al., 2011b). For consistency, we also make sure these landmark curves have the same length. Next we cut open the surface along the two landmark curves. The new surface still has the same geometry but becomes a genus zero surface with two open boundaries. We term this operation as *topological optimization*. The goal is to compute curvilinear coordinates by holomorphic 1-forms (as shown in **Fig. 1** (c)) which introduce a planar surface conformal parameterization. To register hippocampal surfaces, the boundaries serve as landmark curves and are forced to match each other. The computed curvilinear coordinates help apply fluid registration method to align other geometric similar areas. We have applied the topological optimization method in a few of our prior work (Wang et al., 2009a; Wang et al., 2009c; Wang et al., 2011b) and the method can identify these consistent landmark curves. Besides, for quality control purpose, all the hole-labeled meshes were manually checked in this paper. Then the surfaces were conformally mapped to a rectangle plane using holomorphic 1-forms.

We chose to encode surface features using a compound scalar function based on the local conformal factor and the mean curvature: $C(u, v) = \beta \lambda(u, v) + H(u, v)$, where (u, v) is the conformal coordinates of the surface and β is a constant scalar to control the ratio of conformal factor and mean curvature. In the current study, similar to our prior work (Wang et al., 2005a; Wang et al., 2005b), we empirically set β as 7 for both visualization and registration. We then linearly scaled the dynamic range of the conformal representation into $[0, 255]$. With a target image randomly selected, we aligned the deforming images to the target image with the inverse consistent fluid registration method as introduced in Sec. 2.5.

The alignment induced displacements in both u and v directions in the deforming image. We then deformed the corresponding surface with these displacement vectors. After the cross-subject registration was computed with a selected target surface, we calculated the Jacobian matrices J as Eq. 10. The “Log-Euclidean metric” on the set of deformation tensors, \mathcal{S} , was computed as the matrix logarithm $\log(S)$. Since S is a positive-definite matrix, the first 3 of the 4 vector elements, analyzed in mTBM, are the logarithm of the deformation tensor S . We define the multivariate surface morphometry statistic as a 3×1 feature vector consisting of the logged deformation tensors (detailed in Section 2.6).

3.3 Associating Hippocampal Morphometry and Clinical Characteristics

To check the group difference between any two groups (AD vs. MCI, AD vs. control, and control vs. MCI), we performed a group comparison with the Hotelling's T^2 test as Eq. 11 on the 3-dimensional feature vectors. Specifically, for each point on the hippocampal surface, given 0.05 as the significant level, we ran a permutation test with 10,000 random assignments of subjects to groups to estimate the statistical significance of the areas with group differences in surface morphometry. The covariate (group membership) was permuted 10,000 times. The probability was estimated as the ratio of the Mahalanobis distance for a random assignment larger than the group Mahalanobis distance with the true group membership. The probability was later color coded on each surface point as the statistical p -map of group difference. Fig. 6(a)-(c) shows the p -maps of group difference detected between AD and control, AD and MCI, control and MCI groups, respectively, using mTBM as a measure of local surface area change and the significance level at each surface point as 0.05. In Fig. 6, the non-blue color areas denote the statistically significant difference areas between two groups. All group difference p -maps were corrected for multiple comparisons using the widely-used false discovery rate method (FDR) (Benjamini and Hochberg, 1995). The FDR method decides whether a threshold can be assigned to the statistical map that keeps the expected FDR below 5% (i.e., no more than 5% of the voxels are false positive findings). Fig. 6(d)-(f) are the cumulative distribution function (CDF) plots showing the uncorrected p -values (as in a conventional FDR analysis). The x value at which the CDF plot intersects the $y = 20x$ line represents the FDR-corrected p -value or q -value. It is the highest statistical threshold that can be applied to the data, for which at most 5% false positives are expected in the map. In general, a larger q -value indicates a more significant difference in the sense that there is a broader range of statistic threshold that can be used to limit the rate of false positives to at most 5%. The use of the $y = 20x$ line is related to the fact that significance is declared when the volume of suprathreshold statistics is more than 20 times that expected under the null hypothesis (Wang et al., 2011b).

In this experiment, the 194 AD, 402 MCI, and 228 healthy control surfaces were successfully registered by our system. The FDR-corrected p -values for AD vs. control, AD vs. MCI, and control vs. MCI are 0.049, 0.0244, and 0.0483, respectively.

3.4 Diagnostic Group Difference Comparison

In this experiment, we compare our system with the popular surface registration tools FIRST and SPHARM (Styner et al., 2006) in diagnostic group difference detection.

FIRST is an integrated registration and segmentation tool (Patenaude et al., 2011). Before segmentation, FIRST aligns all images onto the MNI152 template with FSL's integrated registration tool, FLIRT. This is a two-stage linear registration process. The first stage is an affine transformation of the whole head to the template with a standard 12 degrees of freedom registration and the second stage achieves a more accurate and robust 12 degrees of freedom registration to the template using a subcortical mask, which is defined in the MNI space. Following the registration, the inverse transformation will be applied to the surface

models to get them into the native image space. The subsequent segmentation will be conducted in the native image space with the original non-interpolated voxel intensities (Patenaude et al., 2011). With the default configuration, we obtained hippocampal surface models generated by FIRST, which are in their native image spaces. We then transformed the surfaces into MNI standard space with the transformation matrices computed by FLIRT. As pointed out in (Patenaude, 2007), applying the original transformation to the mesh in the native image space is equivalent to reconstructing the mesh from the MNI space model. Thus all the surfaces have a common reference frame. The mTBM statistics were computed directly on these registered surfaces given that all the hippocampal surfaces have the same number of vertices and faces and the cross-subject vertex correspondence established by FIRST (Patenaude et al., 2011). It is notable that some prior work (Patenaude, 2007; Carmichael, 2011; Patenaude et al., 2011) also took the established vertex correspondences across subjects by FIRST to study local subcortical structure shape difference between AD patients and healthy controls (Patenaude, 2007; Patenaude et al., 2011) and between patients with learning disabilities and healthy controls (Carmichael, 2011).

SPHARM is another surface mapping tool which is extensively used in the literature (Tae et al., 2011; Alhadidi et al., 2012; Paniagua et al., 2012; Paniagua et al., 2013). It takes binary image segmentation as input and provides functions such as surface extraction, spherical harmonic mapping and surface registration; statistical tools are also included (Styner et al., 2006). In the comparison experiments, we resampled the binary image segmentation processed by FIRST and thresholding as described in Sec. 2.2 with FIRST to generate images with isotropic resolution of $1\text{mm} \times 1\text{mm} \times 1\text{mm}$. The generated isotropic images were used as the input of SPHARM. The parameters used with SPHARM package were set as recommended for hippocampus (Styner et al., 2006). The template was chosen as the same template with the inverse consistent fluid registration. The registered surfaces obtained by SPHARM have the same number of vertices and faces and cross-subject vertex correspondence. We computed the mTBM statistics on these surfaces and generated the significance p -maps. In our experiments, within the dataset that we processed in our fluid registration experiments, 4 AD and 6 MCI subjects failed in SPHARM system either due to segmentation failure or parameterization failure and we excluded them from our experiments. The details of the experiment with SPHARM are discussed in Appendix B.

For performance comparison purpose, **Fig. 7** illustrates the experimental results showing difference maps resulted from the inverse consistent surface fluid registration, FIRST, and SPHARM among the three diagnostic groups (AD, MCI and control) and the CDF plots. In this experiment, considering fairness, we excluded the 4 AD and 6 MCI subjects that failed in SPHARM from the dataset studied by surface fluid and FIRST methods. Thus, 190 AD, 228 controls, 396 MCI subjects were used to compare the surface fluid, FIRST, and SPHARM statistics. MCI is an intermediate stage between the expected cognitive decline of normal aging and the more pronounced decline of dementia. If MCI could be found and treated, the risk of AD will be significantly reduced. However, at MCI stage, changes in brain surface are not significant thus impose more difficulty on the detection. We can see from **Fig. 6** and **Fig. 7** that, in the experimental results, the most prominent results between the proposed method and other methods are in **Fig. 6** (b) and **Fig. 7** (b). **Fig. 6** (b) showed that the new method detected more significant different areas on right side of hippocampus between AD and MCI groups. On the left side, the significant areas are more on lateral zone proximal to the CA1 subfield and superior zone proximal to the combined CA2, CA3, CA4 subfields and gyrus dentatus (GD) (Duvernoy, 1988; Wang et al., 2006). The results agree well with a prior discovery on morphology difference between AD and MCI groups (Morra et al., 2009a), although these two methods used different hippocampal segmentation methods and different surface statistics. Comparing two results, our method detected more significant areas. **Table 1** gives the FDR corrected p -values comparison, which also shows

that our system outperformed two other methods as our method achieved higher FDR corrected p -values.

3.5 Effects of ApoE4 Genotype

The Apolipoprotein E $\epsilon 4$ allele (ApoE4) gene is of special interest in AD analysis as it is the major genetic risk for AD (Poirier et al., 1993; Strittmatter et al., 1993). It has been found that the presence of this allele is more frequent in AD patients than age-matching normal persons and is associated with a younger age of disease onset (Corder et al., 1993; Poirier et al., 1993; Strittmatter et al., 1993; Blacker et al., 1997; Meyer et al., 1998). MRI studies have shown that this allele is associated with greater hippocampal atrophy (Lehtovirta et al., 1995; Geroldi et al., 1999; Hashimoto et al., 2001; Agosta et al., 2009) and one work (Lehtovirta et al., 1995) reported a significant correlation between hippocampal loss and memory deficits. However, only a few studies have investigated the local effect of ApoE4 on hippocampal atrophy in patients of AD/MCI or healthy control subjects (Morra et al., 2009a; Mueller and Weiner, 2009; Qiu et al., 2009b; Pievani et al., 2011). Morra et al. (2009a) discussed that in healthy elderly subjects, presence of ApoE4 may be correlated with future development of AD. In order to investigate this correlation, the authors designed two experiments: (1) group difference between ApoE4 carriers and non-carriers in all samples; (2) group difference between ApoE4 carriers and non-carriers in subjects that have not developed AD, i.e., MCI and control groups. The experiments are aimed to determine if the ApoE4 allele is linked with hippocampal atrophy in all subjects or in just the non-AD subjects. In their study, 400 subjects with 100 AD subjects, 200 MCI subjects, and 100 healthy controls from ADNI baseline data were analyzed with surfaces segmented by a prior work (Morra et al., 2009b). However, no significance was reported in Morra et al. (2009a). Qiu et al. (2009b) studied ApoE4 effects on hippocampal volume and shape in 38 depressed patients without ApoE4, 14 depressed patients with one ApoE4 allele and 31 healthy controls without the ApoE4 allele. They found that the depressed patients with one ApoE4 showed more pronounced shape inward-compression in the anterior CA1 than the depressed patients without the ApoE4 when compared with the healthy controls without the ApoE4. Pievani et al. (2011) designed more systematic experiments to study ApoE4 effects. Their studying subjects include 14 AD patients heterozygous for the ApoE4 allele and 14 patients not carrying the ApoE4 allele and 28 age-, sex-, and education-matched controls. Radial atrophy was analyzed by the same method that used in Morra et al. (2009a). In the group difference study between AD patient ApoE4 carriers and AD non-carriers, they found statistically different atrophy on the left hippocampus but not on the right side.

To study the genetic influence of ApoE4 on hippocampal morphometry, we conducted five sets of experiments that are similar to those studied in (Morra et al., 2009a; Pievani et al., 2011).

1. Group difference between ApoE4 carriers and non-carriers in all subjects;
2. Group difference between ApoE4 carriers and non-carriers in healthy subjects and patients with MCI;
3. Group difference between AD ApoE4 non-carriers and healthy control ApoE4 non-carriers;
4. Group difference between AD ApoE4 carriers and healthy control ApoE4 non-carriers;
5. Group difference between ApoE4 carriers and non-carriers in AD patients.

Fig. 8 shows our experimental results when we used mTBM as the surface statistics. In our study, we used all available samples from ADNI baseline dataset. Among the 824 subjects,

725 subjects have been diagnosed as ApoE4 carriers or non-carriers (366 non-carriers vs. 359 carriers), 558 of which are MCI or controls (310 non-carriers vs. 248 carriers). **Fig. 8(a)** and **(b)** show the significance maps for the two experiments. **Fig. 8(b)** illustrated the results on ApoE4 effects on both healthy control and MCI groups. Our results suggested more significant areas were detected on the left side. The permutation test results showed our method detected significant difference between ApoE4 carriers and ApoE4 non-carriers in healthy subjects and patients with MCI ($p=0.0014$). A few studies to date have investigated ApoE4 effect on the hippocampal atrophy at the subregional level (Morra et al., 2009a; Mueller and Weiner, 2009; Pievani et al., 2011). Among them one study failed to detect an effect (Morra et al., 2009a) and others (Mueller and Weiner, 2009; Pievani et al., 2011) detected effects. However, Mueller and Weiner (2009) investigated a rather small ApoE4 sample ($n=5$ patients) and Pievani et al. (2011) used the manually traced hippocampal contours to segment the hippocampal shape in a small patient data set ($n=28$ patients). Our work is the first study, to our knowledge, which found ApoE4 effect on subregional hippocampal atrophy in healthy subjects and MCI patients in the ADNI dataset. Our method used an automatic image segmentation method to segment hippocampus so our method may have the high throughput advantage. Our results, more significant areas on the left side than on the right side, may also agree with the prior discovery (Pievani et al., 2011) where the effect of ApoE4 mapping was statistically significant on left hippocampus whereas statistically insignificant on the right hippocampus.

Among the 228 healthy controls, 150 subjects are diagnosed as ApoE4 non-carriers; among the 194 AD patients, 56 subjects are diagnosed as ApoE4 non-carriers and 111 subjects ApoE4 carriers. We conducted group difference experiments (3)-(5) among these three groups. **Fig. 8(c)-(e)** show the significance maps of the three experiments. With mTBM, our system detected significant atrophy areas in group difference experiments (1)-(4). In the last experiment (5), our system detected consistent significant areas on the left hippocampus and more significant areas on the right hippocampus than (Pievani et al., 2011), whereas the significant p -value is 0.0581, which is statistically insignificant.

For comparison purpose, we also tested with the other two surface registration methods as in Sec. 3.4. As we mentioned above, we excluded the 4 AD and 6 MCI subjects that failed in SPHARM from our studying dataset used in the surface fluid and FIRST experiments. As a result, among the 814 subjects, 715 subjects have been diagnosed as ApoE4 carriers or non-carriers (360 non-carriers vs. 355 carriers), 552 of which are MCI or controls (306 non-carriers vs. 246 carriers); among the 228 healthy controls, 150 subjects are diagnosed as ApoE4 non-carriers; among the 190 AD patients, 54 subjects are diagnosed as ApoE4 non-carriers and 109 subjects ApoE4 carriers. **Fig. 9** shows the significance p -maps of all five experiments with FIRST as the surface registration method. **Fig. 10** shows the significance p -maps of all five experiments with SPHARM as the surface registration method. The surface fluid registration method on the 814 genetic study dataset gave similar p -maps as **Fig. 8** thus we did not add a figure for it. From **Figs. 8, 9** and **10**, we can find that these three methods generated consistent p -maps. The CDF plots comparisons of the five experiments are shown in **Fig. 11**. The CDF plots are the comparisons of the surface fluid registration, FIRST, and SPHARM on the 814 dataset. From the figure, we can see that our system outperformed FIRST and SPHARM in the third and fourth experiments and obtained comparable results as SPHARM in the first and second experiments. For the fifth experiment, all three methods achieved comparable performance but none was statistically significant when using mTBM as the morphometry statistics.

4. DISCUSSION

The current study has two main contributions. First, we built a subcortical structure surface morphometry system with conformal parameterization and 2D inverse consistent image fluid registration. Pioneering work (Thompson and Toga, 2002; Thompson et al., 2004b) in brain surface registration proposed a cortical pattern matching algorithm to register cortical surfaces by computing a flow field in the cortical parameter space, which matches up corresponding sulci (represented as a set of landmark curves). With surface conformal parameterization (Wang et al., 2007), here we show how the image fluid registration method may be adjusted to enforce appropriate surface correspondences in the parameter domain. We proposed novel surface features, surface conformal representation, to guide the fluid flow to register subcortical surfaces. The proposed surface conformal representation captures both intrinsic surface feature, i.e. conformal factor and extrinsic surface feature, i.e. mean curvature. The surface conformal parameterization was computed by solving a linear system (Wang et al., 2007) so our system is computationally efficient and scalable. Furthermore, due to the simplicity of the Riemannian metric introduced by conformal parameterization, extension of Navier-Stokes equation into general surface space is easy to implement and thus avoids rather complicated Christoffel symbol computation (Thompson et al., 2004b). Our software package together with our multivariate statistic package are publically available at (Wang, 2011). Second, in an open brain imaging dataset, ADNI, we demonstrated ApoE4 is associated with greater atrophy of hippocampal formation in both patients of MCI and healthy control subjects. Our work outperformed the results of a prior work (Morra et al., 2009a) on the same dataset and also validated the observations in Pievani et al. (2011) in a much larger imaging dataset. Our results are related to the concept of preclinical stage AD, a concept that has been validated through autopsy studies (Dickson et al., 1992; Gouras et al., 1997; Bennett et al., 2009; Kok et al., 2009; Caselli et al., 2010), fluorodeoxyglucose positron emission tomography (FDG-PET) studies (Reiman et al., 1996; Reiman et al., 2005) and amyloid ligand binding studies (Reiman et al., 2009) based on the use of Pittsburgh Imaging Compound B (PiB). Our work may provide a structural MRI analysis tool that helps study large numbers of genetically at-risk individuals before the onset of symptomatic memory impairment.

Comparison with SPHARM on synthetic models

The main advantage of our algorithm is the ability to register surface features via a diffeomorphic mapping while preserving the surface topology. To validate the idea, we have conducted a synthetic experiment and compared the result with SPHARM given that the source code of SPHARM is available online. First, we generated a binary volumetric image of a cylinder (**Fig. 12** (a)). The SPHARM image segmentation and surface construction tool generated the surface model (**Fig. 12** (a)). Then, a C-shape was added on the cylinder model at two different locations to simulate the region of interests (ROI) on different surfaces (**Fig. 12** (b)). The combination of the C-shape and the cylindrical surface did not change the vertex number, face number, and connectivity of the original cylindrical surface. Note some staircase effect on the surfaces in **Fig. 12** (b) was introduced from the SPHARM surface construction tool. For a fair comparison, we applied these two surfaces as the input for both SPHARM and our inverse consistent surface fluid registration. As shown in **Fig. 12** (c) and (d), the resulting SPHARM surfaces were reconstructed from the spherical harmonic coefficients, which were computed from the input surfaces and their spherical parameterizations. To show the registration results, we drew the ROI on the study surface with red color and the rest area with blue color. We transferred all the color setting to the template surface via the registration. Presumably, a good registration result will have a clear C-shape (i.e. the ROI) drawn in the red color. In **Fig. 12** (d), we can see that the resulting C-shape is not totally in red, which indicated that the two ROIs were not well aligned. We also

see that some surface features were lost or altered during the reconstruction. On the other hand, as shown in **Fig. 12 (c)**, the C-shape on the template surface is clearly in red and the rest in blue, which indicated that our method was able to well register the regions of interest and keep the surface topology as well. The staircase effect of the input surfaces was well retained in our results. This simple experiment may demonstrate that our method can register surfaces by matching surface features, such as curvature or conformal factor.

Comparison of the inverse consistent fluid registration with/without area distortion correction on synthetic surfaces

Our inverse consistent surface fluid registration method involves solving the Navier-Stokes equation on general manifold. It requires the comparison of vectors at different points on the surface. In general, these vectors are in different tangent planes and we need a way to compare them in a common space (Stam, 2003). On the other hand, parametric surfaces allow tangent vectors to be compared in their parameter domains. To do that, one needs formulate the distortions caused by the surface parameterizations and remedy them by some compensation terms, so we can achieve a set of coordinate invariant differential operators (Stam, 2003; Thompson et al., 2004b; Lui et al., 2005; Wang et al., 2007). Compared with the relatively complicated area distortion compensation terms adopted by some prior work (Stam, 2003; Thompson et al., 2004b), the global conformal parameterization allows a simple formulation using the conformal factor (Lui et al., 2005; Wang et al., 2007). In computer graphics literature (e.g. Stam(2003)), it has been observed that the fluid simulation artifacts were drastically reduced when these compensation terms were applied. To validate if the compensation terms help improve our surface registration quality, we have performed two experiments on the synthetic surface models that have been used in Fig. 5. In our experiments, we applied the inverse consistent surface fluid registration on both directions to register surface 1 to surface 2 (the first row in Fig. 13) and surface 2 to surface 1 (the second row in Fig. 13). We tried to perform the registrations with or without the parameterization compensation terms. We also visualized the pull-back metrics by drawing those equal-spaced black strips defined on the target surfaces back to the source surfaces based on the registration. It is obvious that the registration results with the area distortion correction ((c) and (d)) have more uniform strips than those without the area distortion correction ((e) and (f)). Similar to prior work (Stam, 2003; Thompson et al., 2004b; Lui et al., 2005; Wang et al., 2007), this simple example may help justify our formulation and demonstrate its efficacy to produce a good surface correspondence.

ϵ -Isometric parameterization vs. conformal parameterization

Mathematically speaking, an isometric mapping between two surfaces requires that the first fundamental forms to be equivalent throughout the surfaces whereas a conformal mapping only requires the first fundamental forms to be different by a scalar. As a result, the conditions for conformal mapping are relatively loose. Similar to the cartography problems, it is impossible to compute a mapping from the hippocampal surface to a Euclidean plane that preserves all the geodesic distances. This is a consequence of the theorem of egregium (Do Carmo, 1976): because the Gaussian curvature of the hippocampal surface is nonzero on most of surface areas, whereas the plane has zero curvature, these two surfaces cannot be isometric. In the computer graphics and computer vision fields, there were numerous methods proposed to compute the ϵ -isometric parameterization, i.e. an approximation of isometric mapping, e.g. some methods (Schwartz et al., 1989; Bronstein et al., 2006) apply a multidimensional scaling method (Torgerson, 1952; Shepard, 1962; Kruskal, 1964b; a) to compute the near-isometry mapping to the plane for retinotopic mapping and 3D face recognition study.

On the other hand, conformal parameterization was adopted in various imaging and graphics applications to study surface registration (Lipman and Funkhouser, 2009; Boyer et al., 2011; Wang et al., 2012b). Because of the uniformization theorem, conformal mappings to certain domains exist on every simply connected Riemann surface. The discrete conformal mapping has a rigorous theoretic definition and can be computed accurately. In our study, there exists a conformal mapping from a hippocampal surface with two introduced cuts to the Euclidean plane. Our prior work (Wang et al., 2007) introduced a holomorphic 1-form based method to compute such a conformal mapping. Although there are area distortions on a conformal mapping, considering the definition of conformal factor λ as **Eq. 2**, we can see that conformal factor is a smooth function which describes the stretching effect of conformal parameterization. With the conformal factor as the compensation term, the major novelty of the current work is to introduce the Navier-Stokes equation for Riemann surface by the covariant derivatives. Specifically, in **Eq. 5**, by dividing the conformal factor λ , the flow induced in the parameter domain is adjusted for the area distortion introduced by the conformal parameterization and one may achieve a coordinate invariant PDE solving formulation. The proposed formulation is simpler than the prior work (Thompson and Toga, 2002; Thompson et al., 2004b) and may offer a numerically stable and efficient method for surface registration problem.

Comparison with isometry-based surface registration methods

Many existed isometry-based algorithms have focused on mappings of surfaces to their flattened ones on the Euclidean plane (Timsari and Leahy, 2000; Sander et al., 2001; Zigelman et al., 2002; Balasubramanian et al., 2010). Some research also tried to enforce either distance preserving or near-isometry in the surface registration work (Schreiner et al., 2004; Eckstein et al., 2007; Cho et al., 2011). Among them, Cho et al. (2011) proposed a multi-resolution distortion-minimizing mapping scheme to compute surface correspondence between subcortical surfaces. The same research problem that we are trying to address may justify the effort to briefly compare our work with their work.

In (Cho et al., 2011), although they do not map a hippocampal surface to the Euclidean plane, they employ an area-preserving approximation spherical parameterization method (Shen and Makedon, 2006) to establish an initial surface alignment and, for each iteration, generalize the mapping from the low resolution meshes to high resolution meshes. In the registration step, they formulate the matching problem as an energy minimization problem that is defined on a high-dimensional Riemannian manifold and penalizes the deviation from isometric mapping and triangle flippings. The surface deformation is constrained to move along the source surfaces. Our work formulates the surface registration as an image flow problem so that we convert a 3D registration problem to a 2D one via the conformal parameterization. Because of the nature of 2D image registration, our work is more intuitive and easier to be visualized. Due to the differential covariants, our work compares vector fields and deforms surfaces on their tangent planes and also deforms surfaces on surfaces themselves (both source and target surfaces). Furthermore, the inverse consistent registration framework helps maintain a symmetric correspondence and does not depend on the order we use to compare surfaces. Overall, these two papers take two different approaches, i.e. one projects the matching problem to a high-dimensional Riemannian manifold and pursues an approximated isometry deformation while the other converts the problem to the 2D image plane and solves it with some stable 2D image registration schemes. Although a quantitative comparison may be of interest for future work, two algorithms are comparable and complementary to each other. We expect one method may outperform the other in some contexts but not others, or in some diseases but not others, depending on the type of surfaces to be registered.

Benefits of conformal parameterization

For surface morphometry study, one traditional way to do this is to set up parametric grids on surfaces, which are registered across subjects, and then use differential geometry to come up with useful descriptors of surface features of interest, or to summarize the geometry as a whole. Conformal maps help to induce particularly well-organized grids on surfaces. This simplifies a number of downstream computations of registration and surface metrics. The major benefits of conformal parameterization in our work include: (1) a good initialization alignment. For two similar shapes, their conformal structures are also similar. As a result, the conformal parameterization provides good initial alignments between hippocampal surfaces which are similar in nature; (2) surface conformal representation. It represents both surface intrinsic and extrinsic geometry features; (3) an efficient numerical scheme to solve PDEs on general surfaces. It simplifies the extension of PDEs such as Navier-Stokes equation, to general surface and avoids complicated Christoffel symbol computation (Thompson et al., 2004b). Our work pursues an inverse consistent registration so we need solve the PDEs for multiple times. Therefore, the computational efficiency introduced by the conformal parameterization may help us achieve an efficient and stable solution for surface morphometry study.

System structure design

As a shape analysis software tool, the input to our system is the binarized images, which are obtained either by some automatic image segmentation tools (Morra et al., 2010; Patenaude et al., 2011) or manual segmentation results using some interactive graphic tools (Shattuck and Leahy, 2002; Yushkevich et al., 2006a). In the current paper, we took the input as the automatic segmentation results by FIRST (Patenaude et al., 2011). We generated binary images by thresholding the segmentation results and built surface models for the subsequent surface morphometry analysis. Note other options are also available for such a morphometry system. For example, the FIRST software tool (<http://fsl.fmrib.ox.ac.uk/fsl/fslwiki/FIRST>) generated both images and surface models of subcortical structures. The surface models obtained by FIRST already had cross-subject correspondences and were used in this paper as a comparison method. Whether or not the integrated system provides superior discrimination power than the one working with binarized images still needs more validation. However, the benefit of our current system design is the flexibility for users to adapt the system to different data sources. Furthermore, similar to some other work that used FIRST segmentation results to study relative pose information of subcortical nuclei (Bossa et al., 2011), our software tool may also be interesting to FIRST users so that it may be appealing to a broader range of researchers in the neuroimaging community.

Alternative pipeline consideration

Since the initialization is affected by the mapping, so one may wonder whether it is possible to use a least metric distortion mapping for initialization and then conformal mapping for the fluid flow. The alternative pipeline is appealing but it has some difficulties. First, in our work, similar to M-reps or *cm-rep* work (Pizer et al., 1999; Yushkevich et al., 2006b), we tend to use a cylindrical parameterization for the hippocampus (Wang et al., 2010b; Wang et al., 2011b). Under this setting, it is rare to have two conformally equivalent hippocampal surfaces (i.e. there is a conformal mapping between them) because of the biological variety. As a result, the fluid flow does not generate a conformal mapping in general. Secondly, it is a common belief that a least metric distortion mapping, either defined by explicitly defined landmarks or implicit geometry features, could align anatomical surface for neuroanatomy analysis because functional and architectonic boundaries of the human brain have been linked to the brain structure shapes (Brodmann, 1909). So the current approach, to use

conformal parameterization for initial alignment and refine it with least metric distortion mapping, is indeed a valid and practical approach.

Initial alignment computation

. The initial alignment is important for the success of the proposed surface registration algorithm. Numerous efforts are taken to guarantee good initial alignments between surfaces to be registered. First, all our input data has been registered to the MNI standard space, where all the surfaces have the same orientation. Secondly, we label two consistent landmark curves at the front and back of the hippocampal surface, representing its anterior junction with the amygdala, and its posterior limit as it turns into the white matter of the fornix. They are biologically valid and consistent landmarks across subjects. Given the hippocampal tube-like shape, these landmark curves can be automatically detected by checking the extreme points by searching along the first principle direction of geometric moments of surface (Elad et al., 2004; Zhang and Lu, 2004; Wang et al., 2011b). For the quality control purpose, we have manually checked the consistency of all landmark positions in our current work. Lastly, we parameterize the surfaces to a rectangle by tracing a constant line (iso- u) on the parameter domain. We also make sure the cutting curve passes a geometrically consistent point, e.g. the extreme point on x direction in the MNI standard space. Because the conformal structure is surface intrinsic feature and all hippocampal surfaces have similar shapes, their conformal parametrizations are very similar on the 2D plane. Taken the parameterization as the canonical space, we establish the initial alignment between hippocampal surfaces.

Global affine normalization

In computational neuroanatomy research, brain images are usually transformed into a standardized stereotactic space via a global affine transformation followed by a nonlinear deformation to match the atlas or template, which is a fixed reference coordinate system of the brain. The global affine normalization removes most of the within- and between-subject global differences in brain size. Because global brain size difference does not provide much biological information, these global morphological variabilities should be removed before any localized shape analysis is performed (Chung, 2012). It is a common practice for tensor-based morphometry (TBM) research (Davatzikos et al., 1996; Thompson et al., 2000; Chung et al., 2008; Wang et al., 2010b; Wang et al., 2011b; Wang et al., 2013). In our work, after segmentation, we transformed the segmented hippocampal models into MNI standard space with the transformation matrices computed by FLIRT. Since we use the parameterization space as a common space for registration, this global affine normalization does not affect our registration. The normalization is purely for the following mTBM analysis. It may affect the area or the deformation tensor computation but, by removing the global differences in brain sizes, it provides a stable reference space for hippocampal subfield analysis.

Area distortion compensation and registration regularization terms

There are several coefficients in our formulation (Eqs. 6, 7 and 8). Among them, $\lambda_{f,b}$ are conformal factors and used as the area distortion compensation terms for parametric surface based PDE solving. α , μ and τ are registration regularization terms. Although they are all involved in surface registration, they have different functions. As we discussed, $\lambda_{f,b}$ mainly help achieve coordinate invariant differential operators so that one may solve surface fluid PDEs with parametric surfaces. The benefits to have $\lambda_{f,b}$ are not to achieve an area preserving mapping between 3D surface and parameter domain, instead, they are used to define partial differential operators on manifolds and the covariant differentiation on tensor fields (Do Carmo, 1976). With conformal parameterization, their computation becomes very simple and is only related to conformal factors, $\lambda_{f,b}$. On the other hand, similar to prior work

(Leow et al., 2005a; Chiang et al., 2008), α , μ and τ are registration regularization terms which controls the distortion introduced during the fluid registration. With different settings on these parameters, one may penalize the induced area distortion or enforce smoothness. With these two different regularization terms, our surface fluid registration framework is aimed to achieve a surface registration framework which is both computationally efficient (induced by the conformal parameterization) and produces diffeomorphic surface mappings with controlled distortion (enforced by registration regularization terms).

Inverse consistency for a loss of alignment accuracy?

In our work, inverse consistency is imposed as a constraint. At the initialization, both the forward and backward maps are set as identity maps. They are inverse consistent for sure. But the sum of squared intensity differences (SSD) between the two different images that to be registered will make the whole energy too large to be optimal. Then by changing the forward and backward maps, we gradually reduce the SSD while keeping the inverse consistency of the two maps until the energy cannot be decreased anymore. Here the inverse consistency constraint may even improve the accuracy of the alignment because the two images deform to each other, thus the driving force computed by SSD between them may lead the flows to get more accurate alignments. In summary, besides the fact that it helps a diffeomorphic and balanced surface registration, the inverse consistency does not necessarily sacrifice surface registration accuracy.

Conformal equivalence and conformal factor update

The final deformed map was obtained by first conformally mapping a surface to the parameter domain and second deforming to a template surface by the inverse consistent fluid registration. The former is a conformal mapping and the latter is not a conformal mapping. Since conformal mapping and fluid registration generate diffeomorphic mappings, the surface-to-surface mapping established by our method is a diffeomorphic mapping but usually is not a conformal mapping. To achieve conformal mappings between hippocampal surfaces, the two surfaces have to be conformally equivalent. Generally speaking, two hippocampal surfaces may not be conformally equivalent after we introduce the cuts so the conformal mappings do not always exist. However, we may study the subtle surface difference by studying the conformal structure quotient space - Teichmüller shape space as demonstrated in our prior work (Wang et al., 2009c; Wang et al., 2009b).

As a surface intrinsic feature, the conformal factor is computed after we get the parameterization of the surface and is not adjusted as the map changes. This correction term for fluid registration could make the flow computed in the parameter domain independent of underlying surface metrics, thus the flow directly establishes a mapping between surfaces.

Does the cutting affect the statistics?

To achieve an accurate registration between surfaces, we cut open two landmark curves and convert the landmark matching problem as an explicit boundary matching problem. We have adopted this approach in our prior work on brain cortical surface registration (Wang et al., 2012b) and subcortical surface registration (Wang et al., 2011b). The topology cuts do not change the overall surface geometry because the two sides of the cuts are still in the identical positions. So the cuts do not affect the surface registration and the following shape analysis work. Also since we have the conformal factor as the compensation term for the area distortion in the fluid registration framework, theoretically these cuts should not affect the statistical results on the neighboring regions. As shown in **Fig. 14**, the enlarged figures highlight the positions of the landmark curves and the insignificant regions on the p -map. We can see that the statistically insignificant area does not align exactly with the cutting positions. However, to achieve an accurate surface registration and morphometry analysis,

the cut positions need to be consistent across subjects. Besides the automatic moment-based landmark curve identification method discussed in Sec. 3.2, we also applied a quality control step by manually checking all the cutting positions after the automatic landmark identification step. Although we did not find any inconsistency in this work, we consider that it is a recommended step when applying our pipeline for new analyses.

Visualization of the differences between groups

Here we mainly applied a nonparametric, multivariate permutation testing on Hotelling's T^2 statistics. Compared with the conventional Jacobian determinant (Qiu and Miller, 2008; Qiu et al., 2008; Qiu et al., 2009a; Qiu et al., 2010), the logarithmic transforms are applied to convert the tensors into vectors that are more tractable for Euclidean operations. On the other hand, standard multivariate random field theory may also be applicable to analyze the new multivariate statistics. For instance, in (Worsley et al., 2004; Taylor and Worsley, 2008), results based on random field theory for Roy's maximum root was proposed. The inference for Roy's maximum root is based on the Roy's union-intersection principle (Roy, 1953). Recently, Chung et al. (2010) used this statistic to quantify abnormal local shape variations of the amygdala in 22 high-functioning autistic subjects. Here since we used Hotelling T^2 test, the significant map results are like 2-sided tests and do not carry the direction information. To visualize the deformation directions, we defined a new measurement (Wang et al., 2011a) at each vertex k as

$$R^k = \frac{\sum_i^{N_1} \det J_{1i}^k N_2}{\sum_j^{N_2} \det J_{2j}^k N_1} \quad (12)$$

where J_{1i}^k and J_{2j}^k are the Jacobian matrices for the i th subject in one group and the j th subject in another group, respectively, and N_1 and N_2 are the number of subjects in one group and in another group. The determinant of Jacobian matrix indicates the difference in size of the region in the individual subject compared to the template. When registering the two groups of subjects to a common template, R^k with values greater than 1 indicating that the surface area at that vertex is larger in one group when compared to the other group and vice versa for values smaller than 1. From **Fig. 15** we can see that, when comparing AD patients with healthy controls or MCI subjects and when comparing MCI subjects with healthy controls, as expected, the major area on the hippocampal surface shows atrophy, which represented by the red color. This is also matches the corresponding p -maps as shown in **Fig. 6**. We also observed some enlargements at the anterior and the posterior sides of the surface, which represented by blue color. As pointed out in (Apostolova et al., 2010b), this is probably due to the tissue loss in the neighboring structures of hippocampus, as the anterior and posterior are the junctions with the amygdala and the white matter of the fornix, respectively. As a result, the enlargements may be caused by the shifting of the long axis of the hippocampus.

Clinical significance of surface-based morphometry statistics

Atrophy of brain structures is associated with cognitive impairment in normal aging and AD (Frisoni et al., 2010), and typically results from a combination of neuronal atrophy, cell loss, and impairments in myelin turnover and maintenance, and corresponding reductions in white matter volume. These cellular processes combine at the macroscopic level to induce observable differences on brain MRI. Several of processes (such as cellular atrophy) occur with normal aging, and others (including neuronal loss) are further promoted by amyloid plaque and neurofibrillary tangle deposition. Our work applies mTBM, a surface-based morphometry feature, to study brain structure changes. Although surface expansion and contraction are less traditional measures of morphometry, it is likely that they simply reflect

the same processes that cause progressive brain tissue loss. Our work, as well as some approaches developed by other groups (e.g. Winkler et al. (2010; 2012), Chen et al. (2012), Qiu et al. (2008); Yushkevich (2009)), measure the extent and severity of cortical and hippocampal shape deformations as a proxy for cortical and hippocampal atrophy. The detected expansion or compression of the surface areas are associated with macrostructural and microstructural loss in different brain regions and their association with cognition and genetic influence makes them useful indices of the neurodegenerative process.

Integration of contextual information for hippocampal subfield analysis

Usually surface-based brain imaging approaches (Thompson and Toga, 1996; Fischl et al., 1999; Van Essen et al., 2001; Goebel, 2012) rely on segmented image to build surfaces. They solely use surface geometry information for image registration and shape analysis. Some contextual information is considered in the image segmentation stage and boundaries between two different tissues are determined based on some priors learned from the training data. In hippocampal subfield shape analysis work (Thompson et al., 2004a; Morra et al., 2009a; Qiu et al., 2009b; Apostolova et al., 2010a; Wang et al., 2011b), the morphometry comparison usually only uses geometric information. Some methods (Wang et al., 2003; Wang et al., 2006; Van Leemput et al., 2009; Yassa et al., 2010; Yushkevich et al., 2010) segment hippocampus into different regions and analyze the volume and shape changes of these subfields. These methods compute volumetric image registration between template and individual subject and translate and visualize the deformation on surfaces. We hypothesize the contextual information, e.g. surface registration consider neighboring image information, may improve the registration accuracy. Nonetheless, the integration has many challenges, such as different resolutions, high dimension, etc. How to combine the contextual information, e.g. considering the neighboring image information in the analysis, to improve statistical power still needs further investigation. We noticed some recent work (Du et al., 2011) has proposed new methods which integrate information of curves, surface and volumetric images. It could be a potential future work to improve hippocampal subfield analysis research.

Our algorithm is generic and may be useful for other subcortical structure analysis. There are two main caveats when applying the developed surface fluid registration method to study general subcortical surface registration problem. First, in the topology optimization step, the current algorithm requires two landmark cuts, which may restrict the applicability of the proposed method with other subcortical structures. Thus far, we have applied this algorithm to study putamen morphometry in prematurity study (Shi et al., 2012) and applied another similar algorithm (constrained harmonic map through flattening 3D surfaces (Wang et al., 2011b)) to study morphometry of thalamus (Wang et al., 2011a) and corpus colosum (Wang et al., 2012a) on prematurity and achieved some limited success. Since the subcortical structures are normalized in a common stereotaxic coordinate system in a controlled manner, we assume some geometry extreme positions can serve as geometrically valid and consistent landmarks across subjects in these work. However, it deserves more careful validation on whether these landmarks are also biologically valid and one should be cautious about how consistent they are for a population based study. Second, to map a hippocampal surface to a 2D plane, we introduce a few cuts on the surfaces. Currently, by introducing the same length cuts on consistent surfaces, we try to make sure that the induced boundaries are consistent across surfaces on the parameter domain and the flow computation is the same for vertices that are close to the boundaries as those in the internal areas. Although the cuts may not alter the geometry of the original surface, it could affect the quality of vertex correspondences near the two curves during the surface fluid registration. Even so, it is a logical conclusion from observing the maps in Fig. 14 that the introduced boundaries do not seem to introduce

artifacts and affect the statistical results. It shows the potential of our work for the proposed hippocampal surface morphometry analysis.

5. CONCLUSION

With conformal parameterization, we extended the inverse consistent image fluid registration method to match general surfaces. This has numerous applications in medical imaging. Our examples of matching various hippocampal surfaces are relevant for mapping how degenerative diseases affect the brain, as well as building statistical shape models to detect the anatomical effects of disease, aging, or development. The hippocampus is used as specific examples, but the method is general and is applicable in principle to cortical and other subcortical surfaces.

Our surface-based fluid registration system automates the matching of surfaces by computing a correspondence field guided by the differences of features between the surfaces. This is a natural idea, in that it uses conformal parameterization to transform a surface matching problem into an image registration problem. Whether or not this approach provides a more relevant correspondences than those afforded by other criteria (mutual information, neuralnets, or hand landmarking) requires careful validation for each application. Optimal correspondence depends more on utility for a particular application than on anatomical homology. Because different correspondence principles produced different shape models, we plan to compare them in future work for detecting group differences and genetic influence in brain structures.

As we described in Results section, the inverse consistent fluid flow that matches one surface to another was computed with the surface feature images and the images were computed by summing up local conformal factor and mean curvature and linearly scaling the dynamic range to $[0, 255]$. It is possible that some dynamic ranges in the features will be scaled into just one range in the image. Thus an improvement of the accuracy of the fluid registration is to compute the flow directly on the triangular surface coordinates with the original features and finite element method. We plan to pursue this direction in our future work.

As we discussed in the Results section, our results agree with some literature (Morra et al., 2009a; Pievani et al., 2011). Similar to other surface-based hippocampal subfield analysis work (Thompson et al., 2004a; Morra et al., 2009a; Qiu et al., 2009b; Apostolova et al., 2010a), our method is able to detect some specific significantly different regions. With our current statistical validation strategies, permutation test and false discovery rate, our results match with results from two other methods, SPHARM and FIRST. The spreading results, e.g. between controls and MCI/AD, do not indicate the differences are simply smoothed/averaged over the whole structure. Our future work will further investigate how to apply these detected statistical group differences with drug trials (Gutman et al., 2012), classification (Yuan et al., 2012), and progression (Ye et al., 2012).

In future, we will also apply our inverse consistent surface fluid registration framework to work with other surface features, such as surface heat kernel signature (Sun et al., 2009b), Beltrami coefficients (Lui et al., 2010), etc. The proposed multivariate measures may help in detection of degenerative effects, and may also benefit imaging genetics research (Ho et al., 2010). In this work, we used the group difference study as an application. With multivariate features, it is natural to apply machine learning methods to perform computer-assisted diagnosis and predict future clinical decline (Sun et al., 2009a; Kohannim et al., 2010; Wang et al., 2010a). Our future plan is to incorporate our system with some other machine learning tools, such as support vector machine (Vapnik, 1998), sparse learning (Candès and Tao,

2005), etc., and build a system which may identify imaging biomarkers that are able to evaluate AD related disease burden and predict progression and response to interventions. The combined system may offer a surface-based subcortical structure morphometry tool to detect the anatomical effects on ageing and disease.

Acknowledgments

Data collection and sharing for this project was funded by the Alzheimer's Disease Neuroimaging Initiative (ADNI) (National Institutes of Health Grant U01 AG024904). ADNI is funded by the National Institute on Aging, the National Institute of Biomedical Imaging and Bioengineering, and through generous contributions from the following: Abbott; Alzheimer's Association; Alzheimer's Drug Discovery Foundation; Amorphix Life Sciences Ltd.; AstraZeneca; Bayer HealthCare; BioClinica, Inc.; Biogen Idec Inc.; Bristol-Myers Squibb Company; Eisai Inc.; Elan Pharmaceuticals Inc.; Eli Lilly and Company; F. Hoffmann-La Roche Ltd and its affiliated company Genentech, Inc.; GE Healthcare; Innogenetics, N.V.; Janssen Alzheimer Immunotherapy Research & Development, LLC.; Johnson & Johnson Pharmaceutical Research & Development LLC.; Medpace, Inc.; Merck & Co., Inc.; Meso Scale Diagnostics, LLC.; Novartis Pharmaceuticals Corporation; Pfizer Inc.; Servier; Synarc Inc.; and Takeda Pharmaceutical Company. The Canadian Institutes of Health Research is providing funds to support ADNI clinical sites in Canada. Private sector contributions are facilitated by the Foundation for the National Institutes of Health (www.fnih.org). The grantee organization is the Northern California Institute for Research and Education, and the study is coordinated by the Alzheimer's Disease Cooperative Study at the University of California, San Diego. ADNI data are disseminated by the Laboratory for Neuro Imaging at the University of California, Los Angeles. This research was also supported by NIH grants P30 AG010129, K01 AG030514, and the Dana Foundation.

APPENDIX A

With conformal parameterization, the Riemann metric is defined as:

$$[g_{ij}] = \begin{bmatrix} g_{11} & g_{12} \\ g_{21} & g_{22} \end{bmatrix} = \begin{bmatrix} \lambda & 0 \\ 0 & \lambda \end{bmatrix}$$

The inverse of $[g_{ij}]$ is:

$$[g^{ij}] = \begin{bmatrix} g^{11} & g^{12} \\ g^{21} & g^{22} \end{bmatrix} = \begin{bmatrix} 1/\lambda & 0 \\ 0 & 1/\lambda \end{bmatrix}$$

We now provide the expression in general coordinates of the differential operators that appear in **Eq. 9** (Aris, 1989; Stam, 2003).

Gradient:

$$\nabla_s \varphi = g^{ij} \frac{\partial \varphi}{\partial x_j} = g^{i1} \frac{\partial \varphi}{\partial x_1} + g^{i2} \frac{\partial \varphi}{\partial x_2} = \begin{bmatrix} g^{11} \frac{\partial \varphi}{\partial x_1} + g^{12} \frac{\partial \varphi}{\partial x_2} \\ g^{21} \frac{\partial \varphi}{\partial x_1} + g^{22} \frac{\partial \varphi}{\partial x_2} \end{bmatrix}$$

Thus the gradient operator ∇_s can be written as:

$$\nabla_s = \begin{bmatrix} g^{11} \frac{\partial}{\partial x_1} + g^{12} \frac{\partial}{\partial x_2} \\ g^{21} \frac{\partial}{\partial x_1} + g^{22} \frac{\partial}{\partial x_2} \end{bmatrix}$$

Divergence:

$$\nabla_s \cdot \mathbf{u} = \frac{1}{\sqrt{g}} \frac{\partial}{\partial x_i} (\sqrt{g} u_i) = \frac{1}{\sqrt{g}} \left(\frac{\partial}{\partial x_1} (\sqrt{g} u_1) + \frac{\partial}{\partial x_2} (\sqrt{g} u_2) \right)$$

where $\mathbf{u} = \begin{bmatrix} u_1 \\ u_2 \end{bmatrix}$ and $\sqrt{g} = \sqrt{\det([g_{ij}])} = \sqrt{g_{11}g_{22} - g_{12}g_{21}}$.

The Laplacian can be computed by gradient and divergence as:

$$\Delta_s \varphi = \nabla_s \cdot (\nabla_s \varphi) = \frac{1}{\sqrt{g}} \left(\frac{\partial}{\partial x_1} \left(\sqrt{g} g^{11} \frac{\partial \varphi}{\partial x_1} + \sqrt{g} g^{12} \frac{\partial \varphi}{\partial x_2} \right) + \frac{\partial}{\partial x_2} \left(\sqrt{g} g^{21} \frac{\partial \varphi}{\partial x_1} + \sqrt{g} g^{22} \frac{\partial \varphi}{\partial x_2} \right) \right)$$

Given conformal parameterization $\phi: S \rightarrow \mathbb{R}^2$, where $\sqrt{g} = \lambda$, $g^{11} = g^{22} = \frac{1}{\lambda^2}$, $g^{12} = g^{21} = 0$, we have

$$\Delta_s v = \frac{1}{\lambda} \Delta v$$

For a velocity field $\mathbf{v} = \begin{bmatrix} v_1 \\ v_2 \end{bmatrix}$, $\nabla_s (\nabla_s \cdot \mathbf{v}) = \nabla \left(g^{11} \frac{\partial v_1}{\partial x_1} + g^{12} \frac{\partial v_1}{\partial x_2} + g^{21} \frac{\partial v_2}{\partial x_1} + g^{22} \frac{\partial v_2}{\partial x_2} \right) = \frac{1}{\lambda} \nabla (\nabla \cdot \mathbf{v})$.

APPENDIX B

In details, three commands from SPHARM system were used in sequence:

1. **SegPostProcess**: This command can be used to extract a single label or a label range from the input image, to resample the input image into isotropic resolution, and to ensure the spherical topology of the substructure represented by the image label. Styner et al. (2006) claimed that the input to next command, GenParaMesh has to be of isotropic resolution and a relatively fine resolution is preferred and suggested an isotropic resolution of $0.5 \text{ mm} \times 0.5 \text{ mm} \times 0.5 \text{ mm}$ for hippocampi. However, in our experiment, if we resample the binary images obtained by FIRST with the command SegPostProcess, about 20% of the subjects will fail the following processing. As a result, before running the command, we resampled the binary images into an isotropic resolution of $1 \text{ mm} \times 1 \text{ mm} \times 1 \text{ mm}$ with the linear registration given by FLIRT. Thus, in our comparison experiment, the SegPostProcess command was used as a format conversion tool, i.e., to convert the binary analyze images into a format that can be read by the subsequent commands. The command was run by the following example command line on each isotropic image:

```
SegPostProcessLabel.hdr -o Label_PP.hdr -label 1
```

where Label.hdr is the input and Label_PP.hdr is the output.

2. **GenParaMesh**: This command extracts the surface of the input label segmentation and maps the surface to a sphere with the area-preserving, distortion minimizing spherical mapping (Styner et al., 2006). The command was run by the following example command line:

```
GenParaMeshLabel_PP.hdr -iter 1000 -label 1
```

This command will output two surfaces: Label_PP_surf.meta is the surface and Label_PP_para.meta is the spherical parameterization.

3. ParaToSPHARMMesh: This command computes the SPHARM-PDM representation and resolves issues of correspondence and alignment. The command was run by the following example command line:

```
ParaToSPHARMMeshLabel_PP_surf.metaLabel_PP_para.meta -subdivLevel
10 -spharmDegree 12 - flipTemplatetemplate.coef -
regTemplatetemplate.meta
```

The parameters subdivLevel and spharmDegree were set as recommended for hippocampus (Styner et al., 2006). The flip template was chosen as the same template with the inverse consistent fluid registration and was computed by the above command without providing a flip template. The output of the command will be registered surfaces.

REFERENCE

- Agosta F, Vessel KA, Miller BL, Migliaccio R, Bonasera SJ, Filippi M, Boxer AL, Karydas A, Possin KL, Gorno-Tempini ML. Apolipoprotein E epsilon4 is associated with disease-specific effects on brain atrophy in Alzheimer's disease and frontotemporal dementia. *Proc Natl Acad Sci U S A*. 2009; 106(6):2018–2022. [PubMed: 19164761]
- Alhadidi A, Cevitanes LH, Paniagua B, Cook R, Festy F, Tyndall D. 3D quantification of mandibular asymmetry using the SPHARM-PDM tool box. *Int J Comput Assist Radiol Surg*. 2012; 7(2):265–271. [PubMed: 22089896]
- Apostolova LG, Morra JH, Green AE, Hwang KS, Avedissian C, Woo E, Cummings JL, Toga AW, Jack CR Jr, Weiner MW, Thompson PM. Automated 3D mapping of baseline and 12-month associations between three verbal memory measures and hippocampal atrophy in 490 ADNI subjects. *Neuroimage*. 2010a; 51(1):488–499. [PubMed: 20083211]
- Apostolova LG, Mosconi L, Thompson PM, Green AE, Hwang KS, Ramirez A, Mistur R, Tsui WH, de Leon MJ. Subregional hippocampal atrophy predicts Alzheimer's dementia in the cognitively normal. *Neurobiol Aging*. 2010b; 31(7):1077–1088. [PubMed: 18814937]
- Apostolova LG, Thompson PM, Green AE, Hwang KS, Zoumalan C, Jack CR Jr, Harvey DJ, Petersen RC, Thal LJ, Aisen PS, Toga AW, Cummings JL, Decarli CS. 3D comparison of low, intermediate, and advanced hippocampal atrophy in MCI. *Hum Brain Mapp*. 2010c; 31(5):786–797. [PubMed: 20143386]
- Aris, R. *Vectors, Tensors and the Basic Equations of Fluid Mechanics*. Dover; New York: 1989.
- Arsigny V, Fillard P, Pennec X, Ayache N. Log-Euclidean Metrics for Fast and Simple Calculus on Diffusion Tensors. *Magn. Reson. Med*. 2006; 56(2):411–421. [PubMed: 16788917]
- Ashburner J, Hutton C, Frackowiak R, Johnsrude I, Price C, Friston K. Identifying global anatomical differences: deformation-based morphometry. *Human Brain Mapping*. 1998; 6(5-6):348–357. [PubMed: 9788071]
- Auzias G, Colliot O, Glaunes JA, Perrot M, Mangin JF, Trouve A, Baillet S. Diffeomorphic brain registration under exhaustive sulcal constraints. *IEEE Trans Med Imaging*. 2011; 30(6):1214–1227. [PubMed: 21278014]
- Bajaj CL, Xu G. Anisotropic diffusion of surfaces and functions on surfaces. *ACM Transactions on Graphics*. 2003; 22(1):4–32.
- Bakircioglu M, Joshi S, Miller MI. Landmark Matching on Brain Surfaces via Large Deformation Diffeomorphisms on the Sphere. *Proc. SPIE Medical Imaging*. 1999:710–715.
- Balasubramanian M, Polimeni JR, Schwartz EL. Near-isometric flattening of brain surfaces. *Neuroimage*. 2010; 51(2):694–703. [PubMed: 20149886]
- Benjamini Y, Hochberg Y. Controlling the False Discovery Rate: A Practical and Powerful Approach to Multiple Testing. *Journal of the Royal Statistical Society. Series B (Methodological)*. 1995; 57(1):289–300.
- Bennett DA, De Jager PL, Leurgans SE, Schneider JA. Neuropathologic intermediate phenotypes enhance association to Alzheimer susceptibility alleles. *Neurology*. 2009; 72(17):1495–1503. [PubMed: 19398704]

- Berg L. Clinical Dementia Rating (CDR). *Psychopharmacol Bull.* 1988; 24(4):637–639. [PubMed: 3249765]
- Blacker D, Haines JL, Rodes L, Terwedow H, Go RC, Harrell LE, Perry RT, Bassett SS, Chase G, Meyers D, Albert MS, Tanzi R. ApoE-4 and age at onset of Alzheimer's disease: the NIMH genetics initiative. *Neurology.* 1997; 48(1):139–147. [PubMed: 9008509]
- Bossa M, Zacur E, Olmos S. Statistical analysis of relative pose information of subcortical nuclei: application on ADNI data. *Neuroimage.* 2011; 55(3):999–1008. [PubMed: 21216295]
- Boyer DM, Lipman Y, St Clair E, Puente J, Patel BA, Funkhouser T, Jernvall J, Daubechies I. Algorithms to automatically quantify the geometric similarity of anatomical surfaces. *Proc Natl Acad Sci U S A.* 2011; 108(45):18221–18226. [PubMed: 22025685]
- Bro-Nielsen, M.; Gramkow, C. *Visualization in Biomedical Computing (VBC'96)*. Springer; 1996. Fast fluid registration of medical images.; p. 267-276.
- Brodmann, K. *Vergleichende Lokalisationslehre der Grosshirnrinde in ihren Prinzipien dargestellt auf Grund des Zellenbaues*. Johann Ambrosius Barth Verlag; 1909.
- Bronstein AM, Bronstein MM, Kimmel R. Generalized multidimensional scaling: a framework for isometry-invariant partial surface matching. *Proc Natl Acad Sci U S A.* 2006; 103(5):1168–1172. [PubMed: 16432211]
- Candès EJ, Tao T. Decoding by linear programming. *Information Theory, IEEE Transactions on.* 2005; 51(12):4203–4215.
- Cao J, Worsley KJ. The detection of local shape changes via the geometry of Hotelling's T^2 fields. *Ann. Statist.* 1999; 27(3):925–942.
- Cardenas VA, Chao LL, Studholme C, Yaffe K, Miller BL, Madison C, Buckley ST, Mungas D, Schuff N, Weiner MW. Brain atrophy associated with baseline and longitudinal measures of cognition. *Neurobiol Aging.* 2011; 32(4):572–580. [PubMed: 19446370]
- Carmichael, D. *Hippocampal Volume and Morphometry in a Cognitively Impaired Population at Increased Risk of Schizophrenia: The Edinburgh Study of Comorbidity*. The University of Edinburgh; 2011.
- Caselli RJ, Walker D, Sue L, Sabbagh M, Beach T. Amyloid load in nondemented brains correlates with APOE e4. *Neurosci Lett.* 2010; 473(3):168–171. [PubMed: 20153809]
- Chen CH, Gutierrez ED, Thompson W, Panizzon MS, Jernigan TL, Eyler LT, Fennema-Notestine C, Jak AJ, Neale MC, Franz CE, Lyons MJ, Grant MD, Fischl B, Seidman LJ, Tsuang MT, Kremen WS, Dale AM. Hierarchical genetic organization of human cortical surface area. *Science.* 2012; 335(6076):1634–1636. [PubMed: 22461613]
- Chen K, Reiman EM, Alexander GE, Caselli RJ, Gerkin R, Bandy D, Domb A, Osborne D, Fox N, Crum WR, Saunders AM, Hardy J. Correlations between apolipoprotein E epsilon4 gene dose and whole brain atrophy rates. *Am J Psychiatry.* 2007; 164(6):916–921. [PubMed: 17541051]
- Chiang MC, Leow AD, Klunder AD, Dutton RA, Barysheva M, Rose SE, McMahon KL, de Zubicaray GI, Toga AW, Thompson PM. Fluid registration of diffusion tensor images using information theory. *IEEE Trans Med Imaging.* 2008; 27(4):442–456. [PubMed: 18390342]
- Cho Y, Seong JK, Shin SY, Jeong Y, Kim JH, Qiu A, Im K, Lee JM, Na DL. A multi-resolution scheme for distortion-minimizing mapping between human subcortical structures based on geodesic construction on Riemannian manifolds. *Neuroimage.* 2011; 57(4):1376–1392. [PubMed: 21658456]
- Chou Y-Y, Laporé N, Avedissian C, Madsen SK, Parikshak N, Hua X, Shaw LM, Trojanowski JQ, Weiner MW, Toga AW, Thompson PM. Mapping correlations between ventricular expansion and CSF amyloid and tau biomarkers in 240 subjects with Alzheimer's disease, mild cognitive impairment and elderly controls. *NeuroImage.* 2009; 46(2):394–410. [PubMed: 19236926]
- Chou Y-Y, Laporé N, Saharan P, Madsen SK, Hua X, Jack CR, Shaw LM, Trojanowski JQ, Weiner MW, Toga AW, Thompson PM. Ventricular maps in 804 ADNI subjects: correlations with CSF biomarkers and clinical decline. *Neurobiology of Aging.* 2010; 31(8):1386–1400. [PubMed: 20620663]
- Christensen, GE. *Deformable Shape Models For Anatomy*. Washington University; 1994.
- Christensen GE, Rabbitt RD, Miller MI. Deformable templates using large deformation kinematics. *IEEE Trans Image Process.* 1996; 5(10):1435–1447. [PubMed: 18290061]

- Christensen GE, Johnson HJ. Consistent image registration. *IEEE Trans Med Imaging*. 2001; 20(7): 568–582. [PubMed: 11465464]
- Chung MK, Worsley KJ, Paus T, Cherif C, Collins DL, Giedd JN, Rapoport JL, Evans AC. A unified statistical approach to deformation-based morphometry. *Neuroimage*. 2001; 14:595–606. [PubMed: 11506533]
- Chung MK, Worsley KJ, Robbins S, Paus T, Taylor J, Giedd JN, Rapoport JL, Evans AC. Deformation-based Surface Morphometry Applied to Gray Matter Deformation. *NeuroImage*. 2003; 18:198–213. [PubMed: 12595176]
- Chung MK, Dalton KM, Davidson RJ. Tensor-Based Cortical Surface Morphometry via Weighted Spherical Harmonic Representation. *IEEE Trans. Med. Imag*. 2008; 27(8):1143–1151.
- Chung MK, Worsley KJ, Nacewicz BM, Dalton KM, Davidson RJ. General multivariate linear modeling of surface shapes using SurfStat. *Neuroimage*. 2010; 53(2):491–505. [PubMed: 20620211]
- Chung, MK. *Computational Neuroanatomy: The Methods*. World Scientific Publishing Company; 2012.
- Clarenz U, Diewald U, Rumpf M. Anisotropic Geometric Diffusion in Surface Processing. *IEEE Visualization 2000*. 2000:397–405.
- Corder EH, Saunders AM, Strittmatter WJ, Schmechel DE, Gaskell PC, Small GW, Roses AD, Haines JL, Pericak-Vance MA. Gene dose of apolipoprotein E type 4 allele and the risk of Alzheimer's disease in late onset families. *Science*. 1993; 261(5123):921–923. [PubMed: 8346443]
- Costafreda SG, Dinov ID, Tu Z, Shi Y, Liu CY, Kloszewska I, Mecocci P, Soininen H, Tsolaki M, Vellas B, Wahlund LO, Spenger C, Toga AW, Lovestone S, Simmons A. Automated hippocampal shape analysis predicts the onset of dementia in mild cognitive impairment. *Neuroimage*. 2011; 56(1):212–219. [PubMed: 21272654]
- D'Agostino E, Maes F, Vandermeulen D, Suetens P. A viscous fluid model for multimodal non-rigid image registration using mutual information. *Med Image Anal*. 2003; 7(4):565–575. [PubMed: 14561559]
- Davatzikos C. Spatial Normalization of 3D Brain Images using Deformable Models. *J. Comp. Assisted Tomography*. 1996; 20(4):656–665.
- Davatzikos C, Vaillant M, Resnick SM, Prince JL, Letovsky S, Bryan RN. A computerized approach for morphological analysis of the corpus callosum. *J Comput Assist Tomogr*. 1996; 20(1):88–97. [PubMed: 8576488]
- Davies RH, Twining CJ, Cootes TF, Waterton JC, Taylor CJ. A Minimum Description Length Approach to Statistical Shape Modeling. *IEEE Trans. Med. Imag*. 2002; 21(5):525–537.
- den Heijer T, van der Lijn F, Koudstaal PJ, Hofman A, van der Lugt A, Krestin GP, Niessen WJ, Breteler MMB. A 10-year follow-up of hippocampal volume on magnetic resonance imaging in early dementia and cognitive decline. *Brain*. 2010; 133(4):1163–1172. [PubMed: 20375138]
- Desbrun M, Meyer M, Schröder P, Barr AH. Implicit fairing of irregular meshes using diffusion and curvature flow. *SIGGRAPH '99 Proceedings*. 1999:317–324.
- Desbrun M, Meyer M, Schröder P, Barr AH. Anisotropic Feature-Preserving Denoising of Height Fields and Bivariate Data. *Graphics Interface*. 2000:145–152.
- Dewey J, Hana G, Russell T, Price J, McCaffrey D, Harezlak J, Sem E, Anyanwu JC, Guttman CR, Navia B, Cohen R, Tate DF. Reliability and validity of MRI-based automated volumetry software relative to auto-assisted manual measurement of subcortical structures in HIV-infected patients from a multisite study. *NeuroImage*. 2010; 51(4):1334–1344. [PubMed: 20338250]
- Dickson DW, Crystal HA, Mattiace LA, Masur DM, Blau AD, Davies P, Yen SH, Aronson MK. Identification of normal and pathological aging in prospectively studied nondemented elderly humans. *Neurobiol Aging*. 1992; 13(1):179–189. [PubMed: 1311804]
- Do Carmo, MP. *Differential Geometry of Curves and Surfaces*. Prentice-Hall, Inc.; 1976.
- Du J, Younes L, Qiu A. Whole brain diffeomorphic metric mapping via integration of sulcal and gyral curves, cortical surfaces, and images. *Neuroimage*. 2011; 56(1):162–173. [PubMed: 21281722]
- Durrleman S, Pennec X, Trounev A, Thompson PM, Ayache N. Inferring brain variability from diffeomorphic deformations of currents: An integrative approach. *Medical Image Analysis*. 2008; 12(5):626–637. [PubMed: 18658005]

- Duvernoy, HM. An Atlas of Applied Anatomy. J. F. Bergmann Verlag; Munich: 1988. The Human Hippocampus..
- Eckstein I, Joshi AA, Kuo CC, Leahy R, Desbrun M. Generalized surface flows for deformable registration and cortical matching. *Med Image Comput Assist Interv.* 2007; 10(Pt 1):692–700. [PubMed: 18051119]
- Elad M, Milanfar P, Golub GH. Shape from moments - an estimation theory perspective. *Trans. Sig. Proc.* 2004; 52(7):1814–1829.
- Ferrarini L, Palm WM, Olofsen H, van der Landen R, van Buchem MA, Reiber JHC, Admiraal-Behloul F. Ventricular shape biomarkers for Alzheimer's disease in clinical MR images. *Magnetic resonance in medicine.* 2008; 59(2):260–267. [PubMed: 18228600]
- Fischl B, Sereno MI, Dale AM. Cortical Surface-Based Analysis II: Inflation, Flattening, and a Surface-Based Coordinate System. *NeuroImage.* 1999; 9(2):195–207. [PubMed: 9931269]
- Fleishman S, Drori I, Cohen-Or D. Bilateral mesh denoising. *ACM Transactions on Graphics.* 2003; 22(3):950–953.
- Folstein MF, Folstein SE, McHugh PR. “Mini-mental state”. A practical method for grading the cognitive state of patients for the clinician. *J Psychiatr Res.* 1975; 12(3):189–198. [PubMed: 1202204]
- Fox NC, Scahill RI, Crum WR, Rossor MN. Correlation between rates of brain atrophy and cognitive decline in AD. *Neurology.* 1999; 52(8):1687–1689. [PubMed: 10331700]
- Frisoni GB, Fox NC, Jack CR, Scheltens P, Thompson PM. The clinical use of structural MRI in Alzheimer disease. *Nat Rev Neurol.* 2010; 6(2):67–77. [PubMed: 20139996]
- Geroldi C, Pihlajamaki M, Laakso MP, DeCarli C, Beltramello A, Bianchetti A, Soininen H, Trabucchi M, Frisoni GB. APOE-epsilon4 is associated with less frontal and more medial temporal lobe atrophy in AD. *Neurology.* 1999; 53(8):1825–1832. [PubMed: 10563634]
- Goebel R. BrainVoyager--past, present, future. *Neuroimage.* 2012; 62(2):748–756. [PubMed: 22289803]
- Gouras GK, Relkin NR, Sweeney D, Munoz DG, Mackenzie IR, Gandy S. Increased apolipoprotein E epsilon 4 in epilepsy with senile plaques. *Ann Neurol.* 1997; 41(3):402–404. [PubMed: 9066363]
- Gu, X.; Vemuri, B. *Med Image Comput Assist Interv.* Springer; 2004. Matching 3D shapes using 2D conformal representations.; p. 771-780.
- Gu X, Wang Y, Chan TF, Thompson PM, Yau S-T. Genus zero surface conformal mapping and its application to brain surface mapping. *IEEE Trans. Med. Imag.* 2004a; 23(8):949–958.
- Gu X, Wang Y, Yau S-T. Geometric Compression using Riemann Surface Structure. *Communications in Information and Systems.* 2004b; 3(3):171–182.
- Guggenheimer, HW. *Differential Geometry.* Dover Publications; 1977.
- Gutman BA, Hua X, Rajagopalan P, Chou Y-Y, Wang Y, Yanovsky I, Toga AW, Jack CR Jr. Weiner MW, Thompson PM. Maximizing Power to Track Alzheimer's Disease and MCI Progression by LDA-Based Weighting of Longitudinal Ventricular Surface Features. Submitted to *NeuroImage.* 2012
- Han X, Xu C, Prince JL. A topology preserving level set method for geometric deformable models. *Pattern Analysis and Machine Intelligence. IEEE Transactions on.* 2003; 25(6):755–768.
- Hasboun D, Chantome M, Zouaoui A, Sahel M, Deladoeuille M, Sourour N, Duyme M, Baulac M, Marsault C, Dormont D. MR determination of hippocampal volume: comparison of three methods. *AJNR Am J Neuroradiol.* 1996; 17(6):1091–1098. [PubMed: 8791921]
- Hashimoto M, Yasuda M, Tanimukai S, Matsui M, Hirono N, Kazui H, Mori E. Apolipoprotein E epsilon 4 and the pattern of regional brain atrophy in Alzheimer's disease. *Neurology.* 2001; 57(8):1461–1466. [PubMed: 11673590]
- Hermosillo, G. *Variational methods for multimodal image matching.* Universit  de Nice (INRIA-ROBOTVIS). Sophia Antipolis; France: 2002.
- Hickie I, Naismith S, Ward PB, Turner K, Scott E, Mitchell P, Wilhelm K, Parker G. Reduced hippocampal volumes and memory loss in patients with early- and late-onset depression. *Br J Psychiatry.* 2005; 186:197–202. [PubMed: 15738499]

- Ho AJ, Stein JL, Hua X, Lee S, Hibar DP, Leow AD, Dinov ID, Toga AW, Saykin AJ, Shen L, Foroud T, Pankratz N, Huentelman MJ, Craig DW, Gerber JD, Allen AN, Corneveaux JJ, Stephan DA, DeCarli CS, DeChairo BM, Potkin SG, Jack CR Jr. Weiner MW, Raji CA, Lopez OL, Becker JT, Carmichael OT, Thompson PM. A commonly carried allele of the obesity-related FTO gene is associated with reduced brain volume in the healthy elderly. *Proc Natl Acad Sci U S A*. 2010; 107(18):8404–8409. [PubMed: 20404173]
- Holland D, Brewer JB, Hagler DJ, Fenema-Notestine C, Dale AM. Subregional neuroanatomical change as a biomarker for Alzheimer's disease. *Proc Natl Acad Sci U S A*. 2009; 106(49):20954–20959. [PubMed: 19996185]
- Hoppe, H. Proceedings of the 23rd annual conference on Computer graphics and interactive techniques. ACM; 1996. Progressive meshes.; p. 99-108.
- Hotelling H. The generalization of Student's ratio. *Ann. Math. Statist.* 1931; 2:360–378.
- Hsiung, C-C. A First Course in Differential Geometry. International Press; 1997.
- Hua X, Gutman B, Boyle C, Rajagopalan P, Leow AD, Yanovsky I, Kumar AR, Toga AW, Jack CR Jr. Schuff N, Alexander GE, Chen K, Reiman EM, Weiner MW, Thompson PM. Accurate measurement of brain changes in longitudinal MRI scans using tensor-based morphometry. *Neuroimage*. 2011; 57(1):5–14. [PubMed: 21320612]
- Jack CR Jr. Slomkowski M, Gracon S, Hoover TM, Felmler JP, Stewart K, Xu Y, Shiung M, O'Brien PC, Cha R, Knopman D, Petersen RC. MRI as a biomarker of disease progression in a therapeutic trial of milameline for AD. *Neurology*. 2003; 60(2):253–260. [PubMed: 12552040]
- Jack CR Jr. Shiung MM, Gunter JL, O'Brien PC, Weigand SD, Knopman DS, Boeve BF, Ivnik RJ, Smith GE, Cha RH, Tangalos EG, Petersen RC. Comparison of different MRI brain atrophy rate measures with clinical disease progression in AD. *Neurology*. 2004; 62(4):591–600. [PubMed: 14981176]
- Jones TR, Durand F, Desbrun M. Non-iterative, feature-preserving mesh smoothing. *ACM Transactions on Graphics*. 2003; 22(3):943–949.
- Kim B, Boes JL, Frey KA, Meyer CR. Mutual information for automated unwarping of rat brain autoradiographs. *NeuroImage*. 1997; 5(1):31–40. [PubMed: 9038282]
- Kim WH, Pachauri D, Hatt C, Chung MK, Johnson SC, Singh V. Wavelet based multi-scale shape features on arbitrary surfaces for cortical thickness discrimination *Advances in Neural Information Processing Systems (NIPS)*. 2012:1250–1258.
- Kohannim O, Hua X, Hibar DP, Lee S, Chou YY, Toga AW, Jack CR Jr. Weiner MW, Thompson PM. Boosting power for clinical trials using classifiers based on multiple biomarkers. *Neurobiol Aging*. 2010; 31(8):1429–1442. [PubMed: 20541286]
- Kok E, Haikonen S, Luoto T, Huhtala H, Goebeler S, Haapasalo H, Karhunen PJ. Apolipoprotein E-dependent accumulation of Alzheimer disease-related lesions begins in middle age. *Ann Neurol*. 2009; 65(6):650–657. [PubMed: 19557866]
- Kruskal J. Multidimensional scaling by optimizing goodness of fit to a nonmetric hypothesis. *Psychometrika*. 1964a; 29(1):1–27.
- Kruskal J. Nonmetric multidimensional scaling: A numerical method. *Psychometrika*. 1964b; 29(2): 115–129.
- Lehtovirta M, Laakso MP, Soininen H, Helisalmi S, Mannermaa A, Helkala EL, Partanen K, Ryyanen M, Vainio P, Hartikainen P, et al. Volumes of hippocampus, amygdala and frontal lobe in Alzheimer patients with different apolipoprotein E genotypes. *Neuroscience*. 1995; 67(1):65–72. [PubMed: 7477910]
- Leow A, Huang SC, Geng A, Becker J, Davis S, Toga A, Thompson P. Inverse consistent mapping in 3D deformable image registration: its construction and statistical properties. *Inf Process Med Imaging*. 2005a; 19:493–503. [PubMed: 17354720]
- Leow A, Yu CL, Lee SJ, Huang SC, Protas H, Nicolson R, Hayashi KM, Toga AW, Thompson PM. Brain structural mapping using a novel hybrid implicit/explicit framework based on the level-set method. *NeuroImage*. 2005b; 24(3):910–927. [PubMed: 15652325]
- Leporé N, Brun C, Chou Y-Y, Chiang M-C, Dutton RA, Hayashi KM, Luders E, Lopez OL, Aizenstein HJ, Toga AW, Becker JT, Thompson PM. Generalized Tensor-Based Morphometry of

- HIV/AIDS Using Multivariate Statistics on Deformation Tensors. *IEEE Trans. Med. Imag.* 2008; 27(1):129–141.
- Li Z, Ma L, Jin X, Zheng Z. A new feature-preserving mesh-smoothing algorithm. *The Visual Computer.* 2009; 25(2):139–148.
- Lipman, Y.; Funkhouser, T. *ACM SIGGRAPH 2009 papers.* ACM; New Orleans, Louisiana: 2009. Möbius voting for surface correspondence.; p. 1-12.
- Loop, C. *Smooth Subdivision Surfaces Based on Triangles.* Mathematics Department. University of Utah; 1987.
- Lorensen WE, Cline HE. Marching cubes: A high resolution 3D surface construction algorithm. *SIGGRAPH Comput. Graph.* 1987; 21(4):163–169.
- Lui L, Kwan J, Wang Y, Yau S-T. Computation of Curvatures using Conformal Parameterization. *Communications in Information and Systems.* 2008a; 8(1):1–16.
- Lui LM, Wang Y, Chan TF. Solving PDEs on Manifolds with Global Conformal Parametriaization. *Variational, Geometric, and Level Set Methods in Computer Vision.* 2005:307–319.
- Lui LM, Gu X, Chan TF, Yau S-T. Variational Method on Riemann Surfaces using Conformal Parameterization and its Applications to Image Processing. *Methods Appl. Anal.* 2008b; 15(4): 513–538.
- Lui LM, Wong TW, Thompson P, Chan T, Gu X, Yau ST. Shape-based diffeomorphic registration on hippocampal surfaces using Beltrami holomorphic flow. *Med Image Comput Comput Assist Interv.* 2010; 13(Pt 2):323–330. [PubMed: 20879331]
- Madsen SK, Ho AJ, Hua X, Saharan PS, Toga AW, Jack CR Jr, Weiner MW, Thompson PM. 3D maps localize caudate nucleus atrophy in 400 AD, MCI, and healthy elderly subjects. *Neurobiology of Aging.* 2010; 31(8):1312–1325. [PubMed: 20538376]
- Meyer CR, Boes JL, Kim B, Bland PH, Zasadny KR, Kison PV, Koral K, Frey KA, Wahl RL. Demonstration of accuracy and clinical versatility of mutual information for automatic multimodality image fusion using affine and thin-plate spline warped geometric deformations. *Med Image Anal.* 1997; 1(3):195–206. [PubMed: 9873906]
- Meyer M, Desbrun M, Schröder P, Barr AH. Discrete Differential-Geometry Operators for Triangulated 2-Manifolds. *Proceedings of Visualization and Mathematics.* 2003:35–58.
- Meyer MR, Tschanz JT, Norton MC, Welsh-Bohmer KA, Steffens DC, Wyse BW, Breitner JC. APOE genotype predicts when--not whether--one is predisposed to develop Alzheimer disease. *Nat Genet.* 1998; 19(4):321–322. [PubMed: 9697689]
- Morra JH, Tu Z, Apostolova LG, Green AE, Avedissian C, Madsen SK, Parikshak N, Hua X, Toga AW, Jack CR Jr, Schuff N, Weiner MW, Thompson PM. Automated 3D mapping of hippocampal atrophy and its clinical correlates in 400 subjects with Alzheimer's disease, mild cognitive impairment, and elderly controls. *Hum Brain Mapp.* 2009a; 30(9):2766–2788. [PubMed: 19172649]
- Morra JH, Tu Z, Apostolova LG, Green AE, Avedissian C, Madsen SK, Parikshak N, Toga AW, Jack CR Jr, Schuff N, Weiner MW, Thompson PM. Automated mapping of hippocampal atrophy in 1-year repeat MRI data from 490 subjects with Alzheimer's disease, mild cognitive impairment, and elderly controls. *NeuroImage.* 2009b; 45(1, Supplement 1):S3–S15. [PubMed: 19041724]
- Morra JH, Tu Z, Apostolova LG, Green AE, Toga AW, Thompson PM. Comparison of AdaBoost and Support Vector Machines for Detecting Alzheimer's Disease Through Automated Hippocampal Segmentation. *Medical Imaging, IEEE Transactions on.* 2010; 29(1):30–43.
- Mueller SG, Weiner MW. Selective effect of age, Apo e4, and Alzheimer's disease on hippocampal subfields. *Hippocampus.* 2009; 19(6):558–564. [PubMed: 19405132]
- Ohtake Y, Belyaev AG, Bogaevski IA. Polyhedral Surface Smoothing with Simultaneous Mesh Regularization. *Geometric Modeling and Processing.* 2000:229–237.
- Paniagua B, Bompard L, Cates J, Whitaker R, Datar M, Vachet C, Styner M. Combined SPHARM-PDM and entropy-based particle systems shape analysis framework. *SPIE Conference 8317 Progress in Biomedical Optics and Imaging.* 2012
- Paniagua B, Lyall A, Berger J-B, Vachet C, Hamer R, Woolson S, Lin W, Gilmore J, Styner M. Lateral ventricle morphology analysis via mean latitude axis. *SPIE Conference 8672 Biomedical Applications in Molecular, Structural, and Functional Imaging.* 2013

- Pantazis D, Joshi A, Jiang J, Shattuck DW, Bernstein LE, Damasio H, Leahy RM. Comparison of landmark-based and automatic methods for cortical surface registration. *NeuroImage*. 2010; 49(3):2479–2493. [PubMed: 19796696]
- Patenaude B. *Bayesian Statistical Models of Shape and Appearance for Subcortical Brain Segmentation*. University of Oxford; 2007.
- Patenaude B, Smith SM, Kennedy DN, Jenkinson M. A Bayesian model of shape and appearance for subcortical brain segmentation. *Neuroimage*. 2011; 56(3):907–922. [PubMed: 21352927]
- Pievani M, Galluzzi S, Thompson PM, Rasser PE, Bonetti M, Frisoni GB. APOE4 is associated with greater atrophy of the hippocampal formation in Alzheimer's disease. *Neuroimage*. 2011; 55(3):909–919. [PubMed: 21224004]
- Pitiot A, Delingette H, Toga AW, Thompson PM. Learning object correspondences with the observed transport shape measure. *Inf Process Med Imaging*. 2003; 18:25–37. [PubMed: 15344444]
- Pizer S, Fritsch D, Yushkevich P, Johnson V, Chaney E. Segmentation, registration, and measurement of shape variation via image object shape. *IEEE Trans. Med. Imag*. 1999; 18:851–865.
- Poirier J, Davignon J, Bouthillier D, Kogan S, Bertrand P, Gauthier S. Apolipoprotein E polymorphism and Alzheimer's disease. *Lancet*. 1993; 342(8873):697–699. [PubMed: 8103819]
- Qiu A, Miller MI. Multi-structure network shape analysis via normal surface momentum maps. *NeuroImage*. 2008; 42(4):1430–1438. [PubMed: 18675553]
- Qiu A, Younes L, Miller MI, Csernansky JG. Parallel transport in diffeomorphisms distinguishes the time-dependent pattern of hippocampal surface deformation due to healthy aging and the dementia of the Alzheimer's type. *NeuroImage*. 2008; 40(1):68–76. [PubMed: 18249009]
- Qiu A, Fennema-Notestine C, Dale AM, Miller MI. Regional shape abnormalities in mild cognitive impairment and Alzheimer's disease. *NeuroImage*. 2009a; 45(3):656–661. [PubMed: 19280688]
- Qiu A, Taylor WD, Zhao Z, MacFall JR, Miller MI, Key CR, Payne ME, Steffens DC, Krishnan KR. APOE related hippocampal shape alteration in geriatric depression. *NeuroImage*. 2009b; 44(3):620–626. [PubMed: 19010425]
- Qiu A, Brown T, Fischl B, Ma J, Miller MI. Atlas generation for subcortical and ventricular structures with its applications in shape analysis. *IEEE Trans Image Process*. 2010; 19(6):1539–1547. [PubMed: 20129863]
- Reiman EM, Caselli RJ, Yun LS, Chen K, Bandy D, Minoshima S, Thibodeau SN, Osborne D. Preclinical evidence of Alzheimer's disease in persons homozygous for the epsilon 4 allele for apolipoprotein E. *N Engl J Med*. 1996; 334(12):752–758. [PubMed: 8592548]
- Reiman EM, Chen K, Alexander GE, Caselli RJ, Bandy D, Osborne D, Saunders AM, Hardy J. Correlations between apolipoprotein E epsilon4 gene dose and brain-imaging measurements of regional hypometabolism. *Proc Natl Acad Sci U S A*. 2005; 102(23):8299–8302. [PubMed: 15932949]
- Reiman EM, Chen K, Liu X, Bandy D, Yu M, Lee W, Ayutyanont N, Keppler J, Reeder SA, Langbaum JB, Alexander GE, Klunk WE, Mathis CA, Price JC, Aizenstein HJ, DeKosky ST, Caselli RJ. Fibrillar amyloid-beta burden in cognitively normal people at 3 levels of genetic risk for Alzheimer's disease. *Proc Natl Acad Sci U S A*. 2009; 106(16):6820–6825. [PubMed: 19346482]
- Reuter M, Rosas HD, Fischl B. Highly accurate inverse consistent registration: a robust approach. *Neuroimage*. 2010; 53(4):1181–1196. [PubMed: 20637289]
- Reuter M, Fischl B. Avoiding asymmetry-induced bias in longitudinal image processing. *Neuroimage*. 2011; 57(1):19–21. [PubMed: 21376812]
- Rey D, Subsol G, Delingette H, Ayache N. Automatic detection and segmentation of evolving processes in 3D medical images: Application to multiple sclerosis. *Med Image Anal*. 2002; 6(2):163–179. [PubMed: 12045002]
- Ridha BH, Anderson VM, Barnes J, Boyes RG, Price SL, Rossor MN, Whitwell JL, Jenkins L, Black RS, Grundman M, Fox NC. Volumetric MRI and cognitive measures in Alzheimer disease : comparison of markers of progression. *J Neurol*. 2008; 255(4):567–574. [PubMed: 18274807]
- Roy SN. On a Heuristic Method of Test Construction and its use in Multivariate Analysis. *The Annals of Mathematical Statistics*. 1953; 24(2):220–238.

- Rueckert D, Sonoda LI, Hayes C, Hill DL, Leach MO, Hawkes DJ. Nonrigid registration using free-form deformations: application to breast MR images. *IEEE Trans Med Imaging*. 1999; 18(8): 712–721. [PubMed: 10534053]
- Sander, PV.; Snyder, J.; Gortler, SJ.; Hoppe, H. Proceedings of the 28th annual conference on Computer graphics and interactive techniques. ACM; 2001. Texture mapping progressive meshes.; p. 409-416.
- Schreiner, J.; Asirvatham, A.; Praun, E.; Hoppe, H. ACM SIGGRAPH 2004 Papers. ACM; Los Angeles, California: 2004. Inter-surface mapping.; p. 870-877.
- Schwartz EL, Shaw A, Wolfson E. A Numerical Solution to the Generalized Mapmaker's Problem: Flattening Nonconvex Polyhedral Surfaces. *IEEE Trans. Patt. Anal. Mach. Intell*. 1989; 11(9): 1005–1008.
- Shattuck DW, Leahy RM. BrainSuite: an automated cortical surface identification tool. *Med Image Anal*. 2002; 6(2):129–142. [PubMed: 12045000]
- Shen D, Davatzikos C. HAMMER: hierarchical attribute matching mechanism for elastic registration. *IEEE Trans Med Imaging*. 2002; 21(11):1421–1439. [PubMed: 12575879]
- Shen L, Makedon F. Spherical mapping for processing of 3D closed surfaces. *Image and Vision Computing*. 2006; 24(7):743–761.
- Shepard R. The analysis of proximities: Multidimensional scaling with an unknown distance function. II. *Psychometrika*. 1962; 27(3):219–246.
- Shi, J.; Wang, Y.; Ceschin, R.; An, X.; Nelson, MD.; Panigrahy, A.; Leporé, N. Surface Fluid Registration and Multivariate Tensor-based Morphometry in NewBorns – the Effects of Prematurity on the Putamen.. Asia-Pacific Signal and Information Processing Association Annual Summit and Conference (APSIPA ASC); Hollywood, CA, USA. 2012.
- Shi Y, Morra JH, Thompson PM, Toga AW. Inverse-Consistent Surface Mapping with Laplace-Beltrami Eigen-Features. *Information Processing in Medical Imaging*. 2009:467–478. [PubMed: 19694286]
- Stam J. Flows on surfaces of arbitrary topology. *ACM Transactions on Graphics*. 2003:724–731.
- Stonnington CM, Chu C, Kloppel S, Jack CR Jr, Ashburner J, Frackowiak RS. Predicting clinical scores from magnetic resonance scans in Alzheimer's disease. *Neuroimage*. 2010; 51(4):1405–1413. [PubMed: 20347044]
- Strittmatter WJ, Saunders AM, Schmechel D, Pericak-Vance M, Enghild J, Salvesen GS, Roses AD. Apolipoprotein E: high-avidity binding to beta-amyloid and increased frequency of type 4 allele in late-onset familial Alzheimer disease. *Proc Natl Acad Sci U S A*. 1993; 90(5):1977–1981. [PubMed: 8446617]
- Styner M, Lieberman JA, McClure RK, Weinberger DR, Jones DW, Gerig G. Morphometric analysis of lateral ventricles in schizophrenia and healthy controls regarding genetic and disease-specific factors. *Proc. Natl. Acad. Sci. U. S. A*. 2005; 102(13):4872–4877. [PubMed: 15772166]
- Styner M, Oguz I, Xu S, Brechbühler C, Pantazis D, Levitt JL, Shenton ME, Gerig G. Framework for the Statistical Shape Analysis of Brain Structures using SPHARM-PDM. *Insight Journal*(1071). 2006:242–250.
- Sun D, van Erp TGM, Thompson PM, Bearden CE, Daley M, Kushan L, Hardt ME, Nuechterlein KH, Toga AW, Cannon TD. Elucidating a Magnetic Resonance Imaging-Based Neuroanatomic Biomarker for Psychosis: Classification Analysis Using Probabilistic Brain Atlas and Machine Learning Algorithms. *Biological Psychiatry*. 2009a; 66(11):1055–1060. [PubMed: 19729150]
- Sun, J.; Ovsjanikov, M.; Guibas, L. Proceedings of the Symposium on Geometry Processing. Eurographics Association; Berlin, Germany: 2009b. A concise and provably informative multi-scale signature based on heat diffusion.; p. 1383-1392.
- Sun X, Rosin PL, Martin RR, Langbein FC. Fast and Effective Feature-Preserving Mesh Denoising. *IEEE Transactions on Visualization and Computer Graphics*. 2007; 13(5):925–938. [PubMed: 17622677]
- Sun X, Rosin PL, Martin RR, Langbein FC. Random walks for feature-preserving mesh denoising. *Computer Aided Geometric Design*. 2008; 25(7):437–456.

- Tae WS, Kim SS, Lee KU, Nam EC, Choi JW, Park JI. Hippocampal shape deformation in female patients with unremitting major depressive disorder. *AJNR Am J Neuroradiol*. 2011; 32(4):671–676. [PubMed: 21372170]
- Taubin G. A signal processing approach to fair surface design. *SIGGRAPH '95 Proceedings*. 1995:351–358.
- Taylor JE, Worsley KJ. Random fields of multivariate test statistics, with applications to shape analysis. *Annals of Statistics*. 2008; 36:1–27.
- Thirion JP, Prima S, Subsol G, Roberts N. Statistical analysis of normal and abnormal dissymmetry in volumetric medical images. *Med Image Anal*. 2000; 4(2):111–121. [PubMed: 10972325]
- Thodberg HH. Minimum Description Length shape and appearance models. *Inf Process Med Imaging*. 2003; 18:51–62. [PubMed: 15344446]
- Thompson PM, Toga AW. A surface-based technique for warping 3-dimensional images of the brain. *IEEE Trans. Med. Imag*. 1996; 15(4):1–16.
- Thompson PM, Giedd JN, Woods RP, MacDonald D, Evans AC, Toga AW. Growth Patterns in the Developing Human Brain Detected Using Continuum-Mechanical Tensor Mapping. *Nature*. 2000; 404(6774):190–193. [PubMed: 10724172]
- Thompson PM, Toga AW. A Framework for Computational Anatomy. *Computing and Visualization in Science*. 2002; 5:1–12.
- Thompson PM, Hayashi KM, de Zubicaray GI, Janke AL, Rose SE, Semple J, Hong MS, Herman DH, Gravano D, Doddrell DM, Toga AW. Mapping hippocampal and ventricular change in Alzheimer's disease. *NeuroImage*. 2004a; 22(4):1754–1766. [PubMed: 15275931]
- Thompson PM, Hayashi KM, Sowell ER, Gogtay N, Giedd JN, Rapoport JL, de Zubicaray GI, Janke AL, Rose SE, Semple J, Doddrell DM, Wang Y, van Erp TGM, Cannon TD, Toga AW. Mapping cortical change in Alzheimer's disease, brain development, and schizophrenia. *NeuroImage*. 2004b; 23(Supplement 1):S2–S18. [PubMed: 15501091]
- Timsari B, Leahy RM. Optimization method for creating semi-isometric flat maps of the cerebral cortex. *Medical Imaging 2000: Image Processing*. 2000; 3979(1):698–708.
- Torgerson W. Multidimensional scaling: I. Theory and method. *Psychometrika*. 1952; 17(4):401–419.
- Vaillant M, Glaunes J. Surface matching via currents. *Inf Process Med Imaging*. 2005; 19:381–392. [PubMed: 17354711]
- Vaillant M, Qiu A, Glaunes J, Miller MI. Diffeomorphic metric surface mapping in subregion of the superior temporal gyrus. *Neuroimage*. 2007; 34(3):1149–1159. [PubMed: 17185000]
- Van Essen DC, Drury HA, Dickson J, Harwell J, Hanlon D, Anderson CH. An Integrated Software Suite for Surface-based Analyses of Cerebral Cortex. *J Am Med Inform Assoc*. 2001; 8(5):443–459. [PubMed: 11522765]
- Van Leemput K, Bakkour A, Benner T, Wiggins G, Wald LL, Augustinack J, Dickerson BC, Golland P, Fischl B. Automated segmentation of hippocampal subfields from ultra-high resolution in vivo MRI. *Hippocampus*. 2009; 19(6):549–557. [PubMed: 19405131]
- Vapnik, V. *Statistical Learning Theory*. Wiley-Interscience; New York: 1998.
- Wang L, Swank JS, Glick IE, Gado MH, Miller MI, Morris JC, Csernansky JG. Changes in hippocampal volume and shape across time distinguish dementia of the Alzheimer type from healthy aging. *NeuroImage*. 2003; 20(2):667–682. [PubMed: 14568443]
- Wang L, Miller JP, Gado MH, McKeel DW, Rothermich M, Miller MI, Morris JC, Csernansky JG. Abnormalities of hippocampal surface structure in very mild dementia of the Alzheimer type. *Neuroimage*. 2006; 30(1):52–60. [PubMed: 16243546]
- Wang Y, Chiang M-C, Thompson PM. Automated Surface Matching using Mutual Information Applied to Riemann Surface Structures. *Med. Image Comp. Comput.-Assist. Intervention, Proceedings, Part II*. 2005a:666–674.
- Wang, Y.; Chiang, M-C.; Thompson, PM. Proceedings of the Tenth IEEE International Conference on Computer Vision (ICCV'05) Volume 1 - Volume 01. IEEE Computer Society; 2005b. Mutual Information-Based 3D Surface Matching with Applications to Face Recognition and Brain Mapping.; p. 527-534.

- Wang Y, Lui LM, Gu X, Hayashi KM, Chan TF, Toga AW, Thompson PM, Yau S-T. Brain Surface Conformal Parameterization using Riemann Surface Structure. *IEEE Trans. Med. Imag.* 2007; 26(6):853–865.
- Wang Y, Yin X, Zhang J, Gu X, Chan TF, Thompson PM, Yau S-T. Brain Mapping with the Ricci Flow Conformal Parameterization and Multivariate Statistics on Deformation Tensors. 2nd MICCAI Workshop on Mathematical Foundations of Computational Anatomy. 2008:36–47.
- Wang Y, Chan TF, Toga AW, Thompson PM. Multivariate Tensor-based Brain Anatomical Surface Morphometry via Holomorphic One-Forms. *Med. Image Comp. Comput.-Assist. Intervention, Proceedings.* 2009a; 12(Pt 1):337–344.
- Wang Y, Dai W, Gu X, Chan TF, Yau ST, Toga AW, Thompson PM. Teichmüller shape space theory and its application to brain morphometry. *Med Image Comput Comput Assist Interv.* 2009b; 12(Pt 2):133–140. [PubMed: 20426105]
- Wang Y, Gu X, Chan TF, Thompson PM. Shape Analysis with Conformal Invariants for Multiply Connected Domains and its Application to Analyzing Brain Morphology. *IEEE Conf. Comp. Vis. Patt. Recog. CVPR '09.* 2009c:202–209.
- Wang, Y.; Senstad, R.; Toga, AW.; Thompson, PM. MRI-based Biomarker Detection using Conformal Slit Maps and Machine Learning.. The 16th Annual Meeting of the Organization for Human Brain Mapping; Barcelona, Spain. 2010a.
- Wang Y, Zhang J, Gutman B, Chan TF, Becker JT, Aizenstein HJ, Lopez OL, Tamburo RJ, Toga AW, Thompson PM. Multivariate tensor-based morphometry on surfaces: Application to mapping ventricular abnormalities in HIV/AIDS. *NeuroImage.* 2010b; 49(3):2141–2157. [PubMed: 19900560]
- Wang, Y. Multivariate Surface-based Subcortical Structure Morphometry System. 2011. Available from: <http://gsl.lab.asu.edu/conformal.htm>
- Wang, Y.; Panigrahy, A.; Shi, J.; Ceschin, R.; Nelson, M.; Gutman, B.; Thompson, P.; Leporé, N. Surface Multivariate Tensor-based Morphometry on Premature Neonates: A Pilot Study. *Image Analysis of Human Brain Development (IAHBD)*; Toronto, Canada: 2011a.
- Wang Y, Song Y, Rajagopalan P, An T, Liu K, Chou YY, Gutman B, Toga AW, Thompson PM. Surface-based TBM boosts power to detect disease effects on the brain: An N=804 ADNI study. *Neuroimage.* 2011b; 56(4):1993–2010. [PubMed: 21440071]
- Wang, Y.; Panigrahy, A.; Shi, J.; Ceschin, R.; Nie, Z.; Nelson, MD.; Leporé, N. 3D vs. 2D Surface Shape Analysis of the Corpus Collosum in Premature Neonates.. *MICCAI: Workshop on Paediatric and Perinatal Imaging*; Nice, France. 2012a.
- Wang Y, Shi J, Yin X, Gu X, Chan TF, Yau S-T, Toga AW, Thompson PM. Brain Surface Conformal Parameterization with the Ricci Flow. *IEEE Trans. Med. Imag.* 2012b; 31(2):251–264.
- Wang Y, Yuan L, Shi J, Greve A, Ye J, Toga AW, Reiss AL, Thompson PM. Applying Tensor-based Morphometry to Parametric Surfaces can Improve MRI-based Disease Detection and Classification. *NeuroImage.* 2013 In Press.
- Wechsler, D. Wechsler Memory Scale-Revised Manual. Psychological Corporation; San Antonio, TX: 1987.
- West J, Fitzpatrick JM, Wang MY, Dawant BM, Maurer CR Jr, Kessler RM, Maciunas RJ, Barillot C, Lemoine D, Collignon A, Maes F, Suetens P, Vandermeulen D, van den Elsen PA, Napel S, Sumanaweera TS, Harkness B, Hemler PF, Hill DL, Hawkes DJ, Studholme C, Maintz JB, Viergever MA, Malandain G, Woods RP, et al. Comparison and evaluation of retrospective intermodality brain image registration techniques. *J Comput Assist Tomogr.* 1997; 21(4):554–566. [PubMed: 9216759]
- Winkler AM, Kochunov P, Blangero J, Almasy L, Zilles K, Fox PT, Duggirala R, Glahn DC. Cortical thickness or grey matter volume? The importance of selecting the phenotype for imaging genetics studies. *NeuroImage.* 2010; 53(3):1135–1146. [PubMed: 20006715]
- Winkler AM, Sabuncu MR, Yeo BT, Fischl B, Greve DN, Kochunov P, Nichols TE, Blangero J, Glahn DC. Measuring and comparing brain cortical surface area and other areal quantities. *Neuroimage.* 2012; 61(4):1428–1443. [PubMed: 22446492]

- Wolz R, Heckemann RA, Aljabar P, Hajnal JV, Hammers A, Lötjönen J, Rueckert D. Measurement of hippocampal atrophy using 4D graph-cut segmentation: Application to ADNI. *NeuroImage*. 2010; 52(1):109–118. [PubMed: 20382238]
- Worsley KJ, Taylor JE, Tomaiuolo F, Lerch J. Unified univariate and multivariate random field theory. *Neuroimage*. 2004; 23(Suppl 1):S189–195. [PubMed: 15501088]
- Yanovsky I, Leow AD, Lee S, Osher SJ, Thompson PM. Comparing registration methods for mapping brain change using tensor-based morphometry. *Med Image Anal*. 2009; 13(5):679–700. [PubMed: 19631572]
- Yassa MA, Stark SM, Bakker A, Albert MS, Gallagher M, Stark CE. High-resolution structural and functional MRI of hippocampal CA3 and dentate gyrus in patients with amnesic Mild Cognitive Impairment. *Neuroimage*. 2010; 51(3):1242–1252. [PubMed: 20338246]
- Ye J, Farnum M, Yang E, Verbeek R, Lobanov V, Raghavan N, Novak G, Dibernardo A, Narayan VA. Sparse learning and stability selection for predicting MCI to AD conversion using baseline ADNI data. *BMC Neurol*. 2012; 12(1):46. [PubMed: 22731740]
- Yeo BT, Sabuncu MR, Vercauteren T, Ayache N, Fischl B, Golland P. Spherical demons: fast diffeomorphic landmark-free surface registration. *IEEE Trans Med Imaging*. 2010; 29(3):650–668. [PubMed: 19709963]
- Ystad MA, Lundervold AJ, Wehling E, Espeseth T, Rootwelt H, Westlye LT, Andersson M, Adolfsdottir S, Geitung JT, Fjell AM, Reinvang I, Lundervold A. Hippocampal volumes are important predictors for memory function in elderly women. *BMC Med Imaging*. 2009; 9:17. [PubMed: 19698138]
- Yuan L, Wang Y, Thompson PM, Narayan VA, Ye J. Multi-source feature learning for joint analysis of incomplete multiple heterogeneous neuroimaging data. *Neuroimage*. 2012; 61(3):622–632. [PubMed: 22498655]
- Yushkevich PA, Piven J, Hazlett HC, Smith RG, Ho S, Gee JC, Gerig G. User-guided 3D active contour segmentation of anatomical structures: significantly improved efficiency and reliability. *Neuroimage*. 2006a; 31(3):1116–1128. [PubMed: 16545965]
- Yushkevich PA, Zhang H, Gee JC. Continuous medial representation for anatomical structures. *IEEE Trans Med Imaging*. 2006b; 25(12):1547–1564. [PubMed: 17167991]
- Yushkevich PA. Continuous medial representation of brain structures using the biharmonic PDE. *NeuroImage*. 2009; 45(1 Suppl):S99–110. [PubMed: 19059348]
- Yushkevich PA, Wang H, Pluta J, Das SR, Craige C, Avants BB, Weiner MW, Mueller S. Nearly automatic segmentation of hippocampal subfields in in vivo focal T2-weighted MRI. *Neuroimage*. 2010; 53(4):1208–1224. [PubMed: 20600984]
- Zhang D, Lu G. Review of shape representation and description techniques. *Pattern Recognition*. 2004; 37(1):1–19.
- Zhang H, Fiume E. Mesh Smoothing with Shape or Feature Preservation. *Advances in Modeling, Animation, and Rendering*. 2002:167–182.
- Zhong J, Qiu A. Multi-manifold diffeomorphic metric mapping for aligning cortical hemispheric surfaces. *NeuroImage*. 2010; 49(1):355–365. [PubMed: 19698793]
- Zigelman G, Kimmel R, Kiryati N. Texture mapping using surface flattening via multidimensional scaling. *Visualization and Computer Graphics, IEEE Transactions on*. 2002; 8(2):198–207.

Highlights

- Efficient formulation of manifold fluid registration by conformal parameterization
- An inverse consistent non-linear surface registration scheme
- Surface multivariate TBM was adopted as morphometry statistics in the system
- The system achieved better performance than some other surface registration tools
- ApoE4 may be associated with accelerated brain atrophy on MCI patients and controls

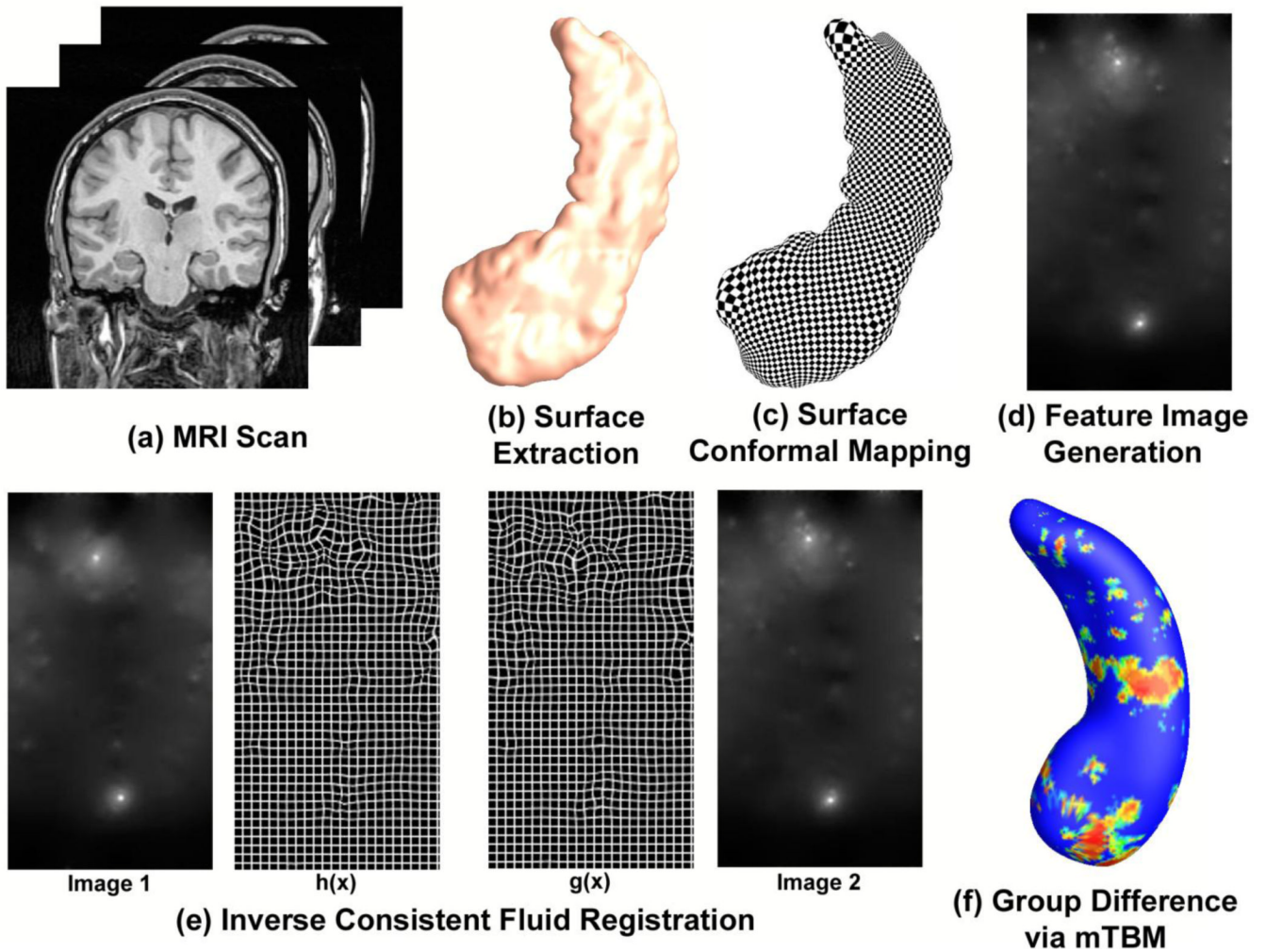


Figure 1.

A segmentation and surface construction chart showing the key steps in our system. After the hippocampal surfaces were extracted from MRI scans automatically with FIRST, we computed their conformal parameterization with holomorphic 1-forms. Then feature images were generated by combining the local conformal factor and mean curvature that were computed from the conformal parameterizations. After the inverse consistent fluid registration was done in the feature image domain, we deformed the surfaces using the obtained displacements. The statistics of multivariate TBM were computed at each point on the resultant matching surface. Then the Hotelling T^2 test was applied to compute differences between two different groups.

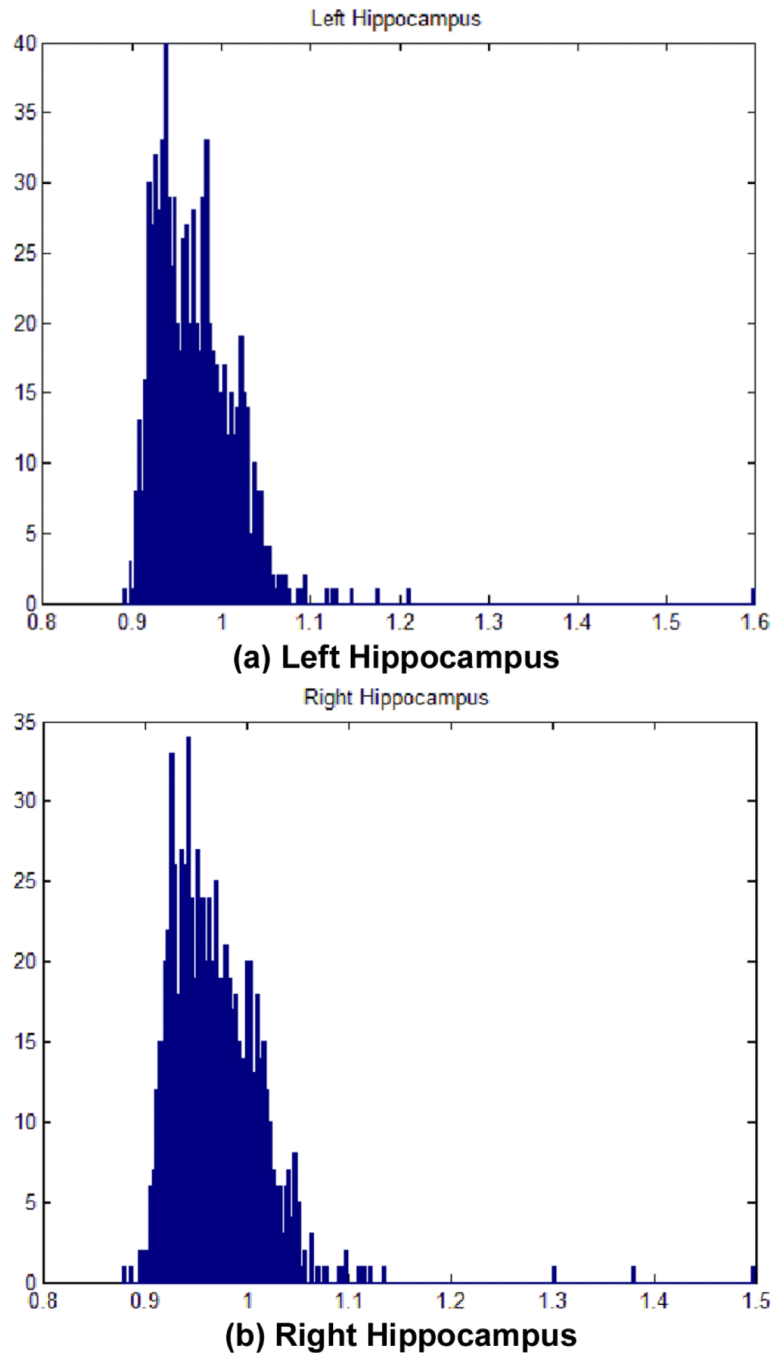
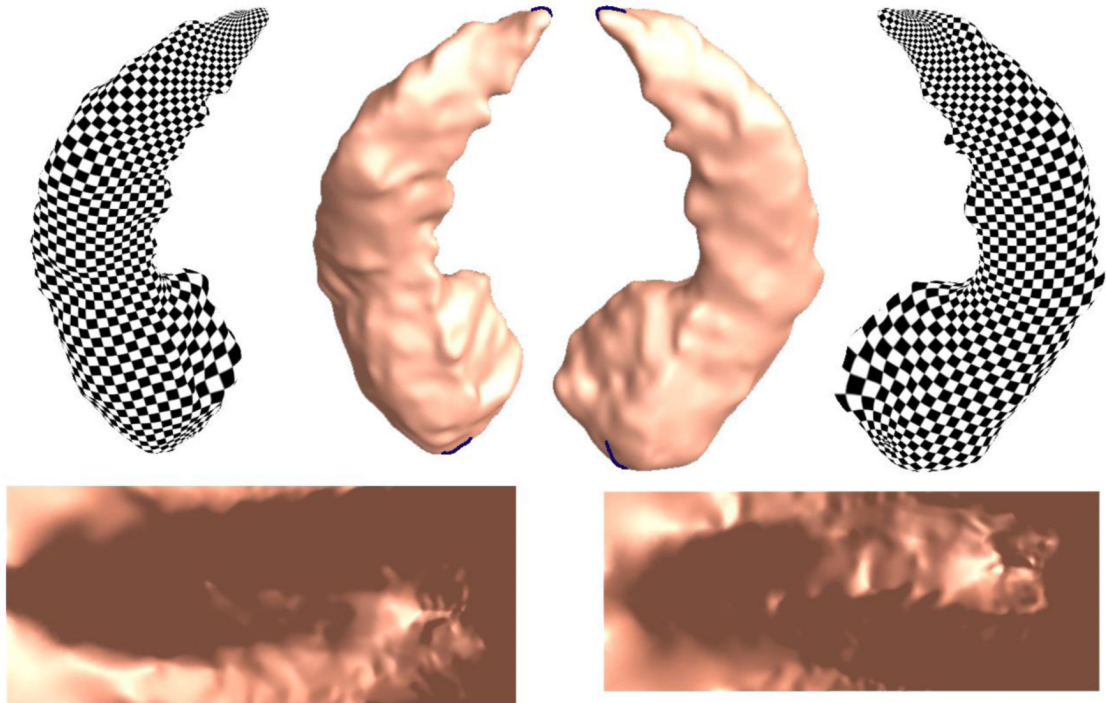
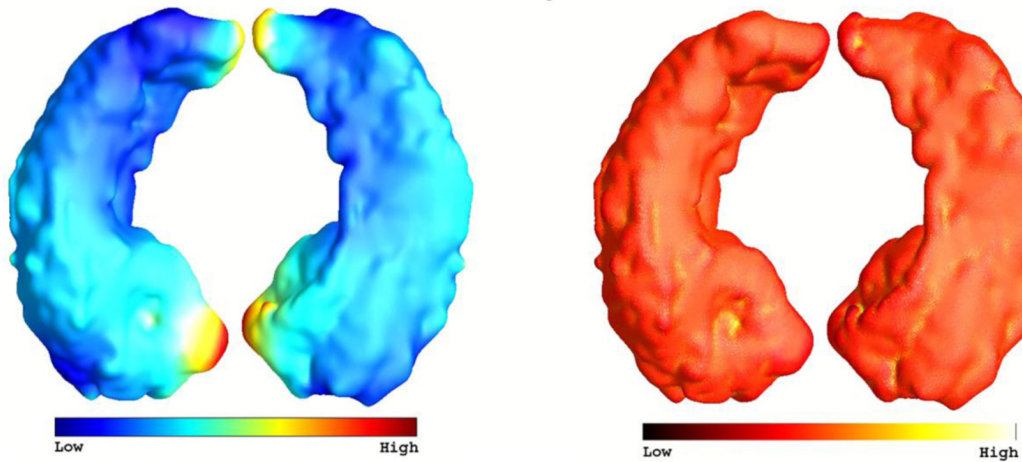


Figure 2.

Histogram showing the Hausdorff distances between the smoothed meshes and original meshes. The majority of the absolute distances fall into the range [0.9, 1.1] with the unit as millimeter. Given the volumes of hippocampus lie between 3000 and 4000 mm^3 (Hasboun et al., 1996; Hickie et al., 2005; Ystad et al., 2009; Carmichael, 2011), our smoothed meshes can be regarded as accurate approximations of the original surfaces.



(a) Conformal Parameterization of Hippocampus with Holomorphic 1-Forms



(b) Conformal Factor and Mean Curvature

Figure 3.

Illustration of surface conformal parameterization (a) and geometric features (b). In (a), the boundaries generated in the topology optimization step were labeled in blue color. Each side of the hippocampal surface was conformally mapped to a rectangle in the parameter domain. The overlaid checkboard texture is used to demonstrate angle preserving property; the shading effect on the parameter space was generated by rendering the original 3D surface with the surface normal directions on each point. In (b), surface geometric features were color coded. The parameterization results and geometric features were used for surface registration and morphometric analysis.

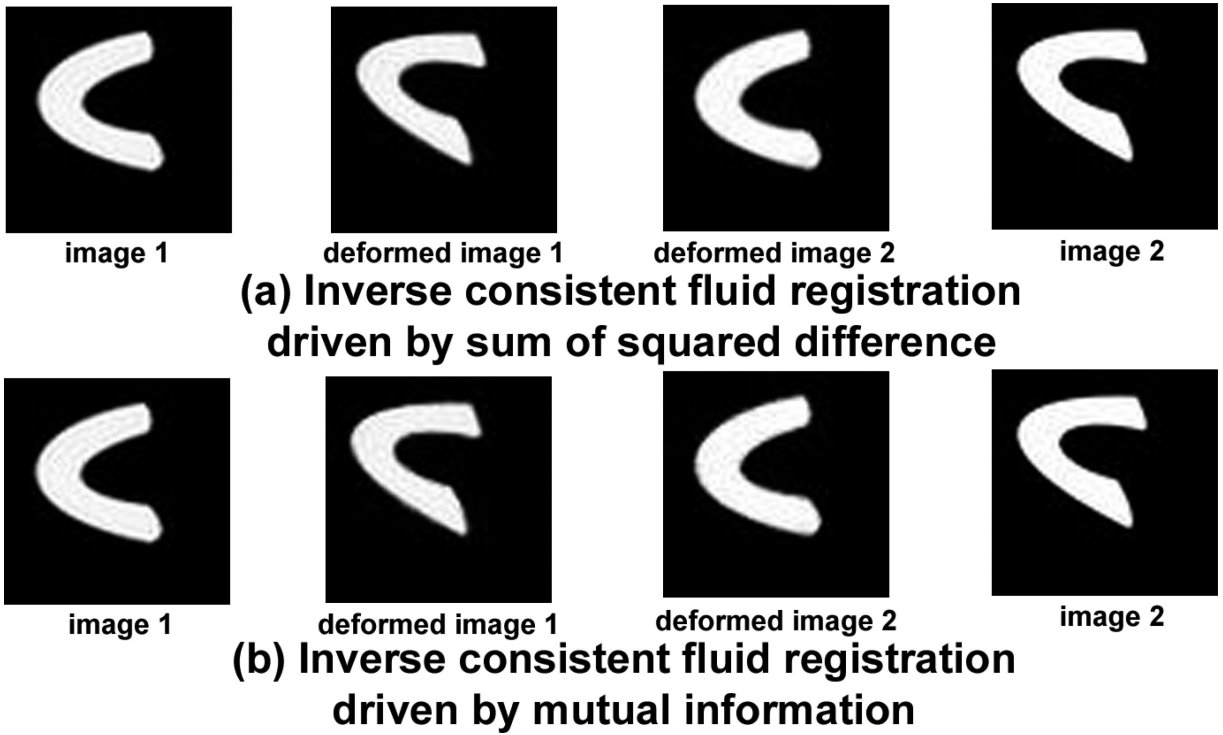


Figure 4.

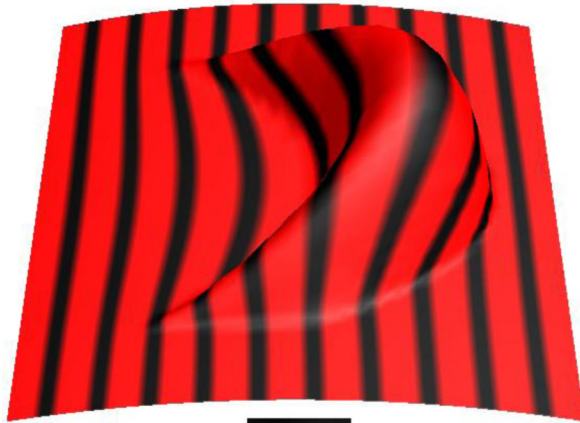
Inverse consistent fluid registration driven by sum of squared intensity difference (SSD) (a) and mutual information (MI) (b) respectively on synthetic images to demonstrate the efficiency of SSD. Although the registration results were similar, the SSD based method took 14.15 seconds while the MI based method took 1730.15 seconds.



(a) Synthetic Surface 1 and Its Feature Image



(c) Deformed Surface 1 and Deformed Feature Image



(b) Synthetic Surface 2 and Its Feature Image



(d) Deformed Surface 2 and Deformed Feature Image

Inverse Consistent Fluid Registration on Synthetic Surfaces

Figure 5.

Matching of geometric features in the 2D parameter domain with the inverse consistent fluid registration of two synthetic surfaces. With the forward and backward mappings obtained in the parameter domain, we induced a forward deformation and a backward deformation in surface 1 and surface 2, respectively. As we can see from (c) and (d), without changing the shape of the surfaces, the features on them are well aligned to each other.

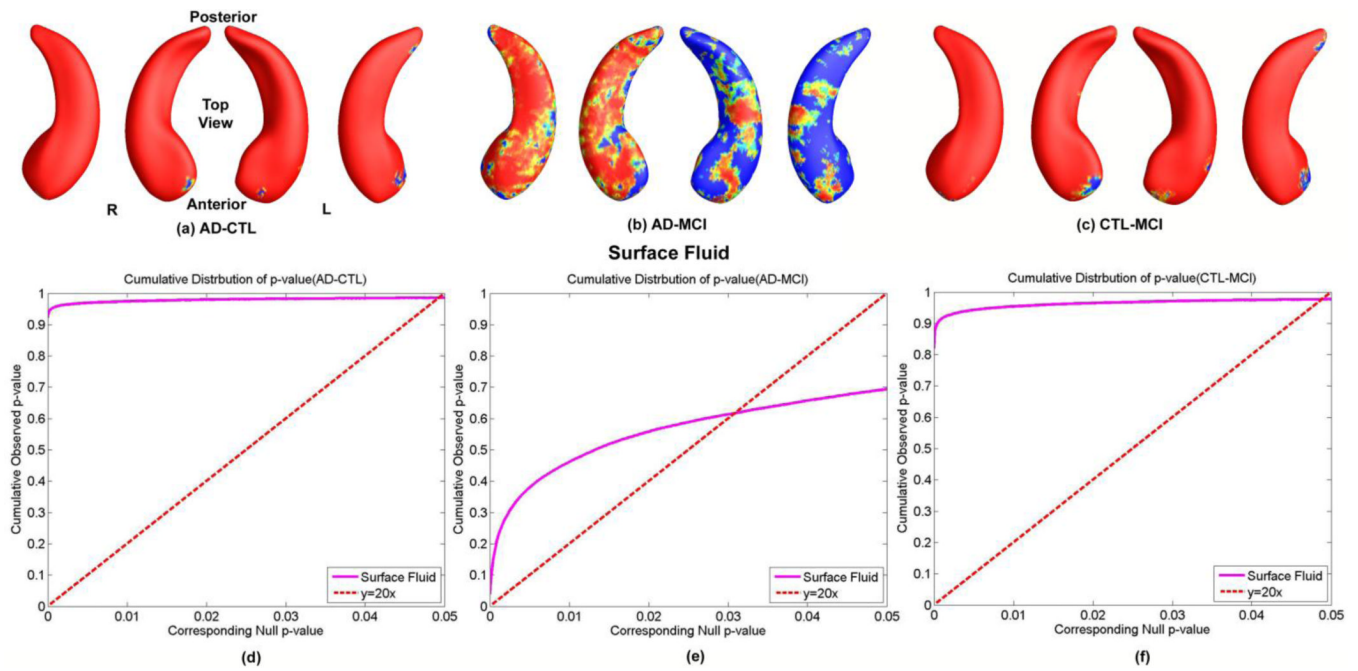


Figure 6. Illustration of inverse consistent surface fluid registration on map of local shape differences (p -values) between different diagnostic groups, based on the multivariate TBM method with hippocampal surfaces from ADNI baseline dataset, which were automatically segmented by FIRST. (a), (b), (c) are group difference p -maps between AD and control, AD and MCI, MCI and control, respectively, in 194 AD, 402 MCI, and 228 control subjects. The p -map color scale is the same as Fig. 8. (d), (e), (f) are the CDF plots.

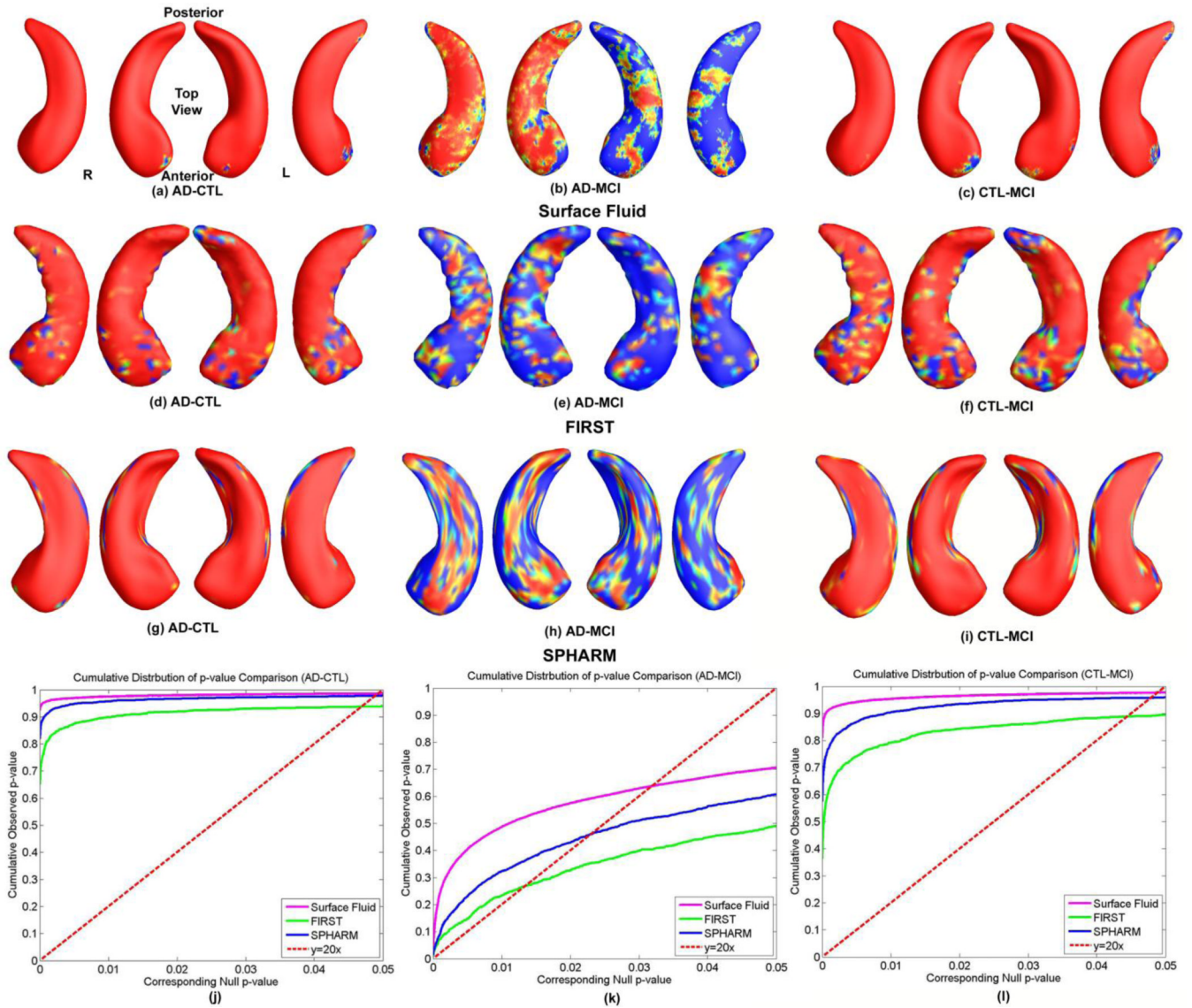


Figure 7. Illustration of comparisons of inverse consistent surface fluid registration with FIRST and SPHARM on map of local shape differences (p -values) between different diagnostic groups, based on the multivariate TBM method with hippocampal surfaces from ADNI baseline dataset, which were automatically segmented by FIRST. (a), (b), (c) are results of our method, (d), (e), (f) are result of FIRST, (g), (h), (i) are results of SPHARM on group difference between AD and control, AD and MCI, MCI and control, respectively, in 190 AD, 396 MCI, and 228 control subjects. The p -map color scale is the same as Fig. 8. (j), (k), (l) are the CDF plots showing the comparisons of the three methods.

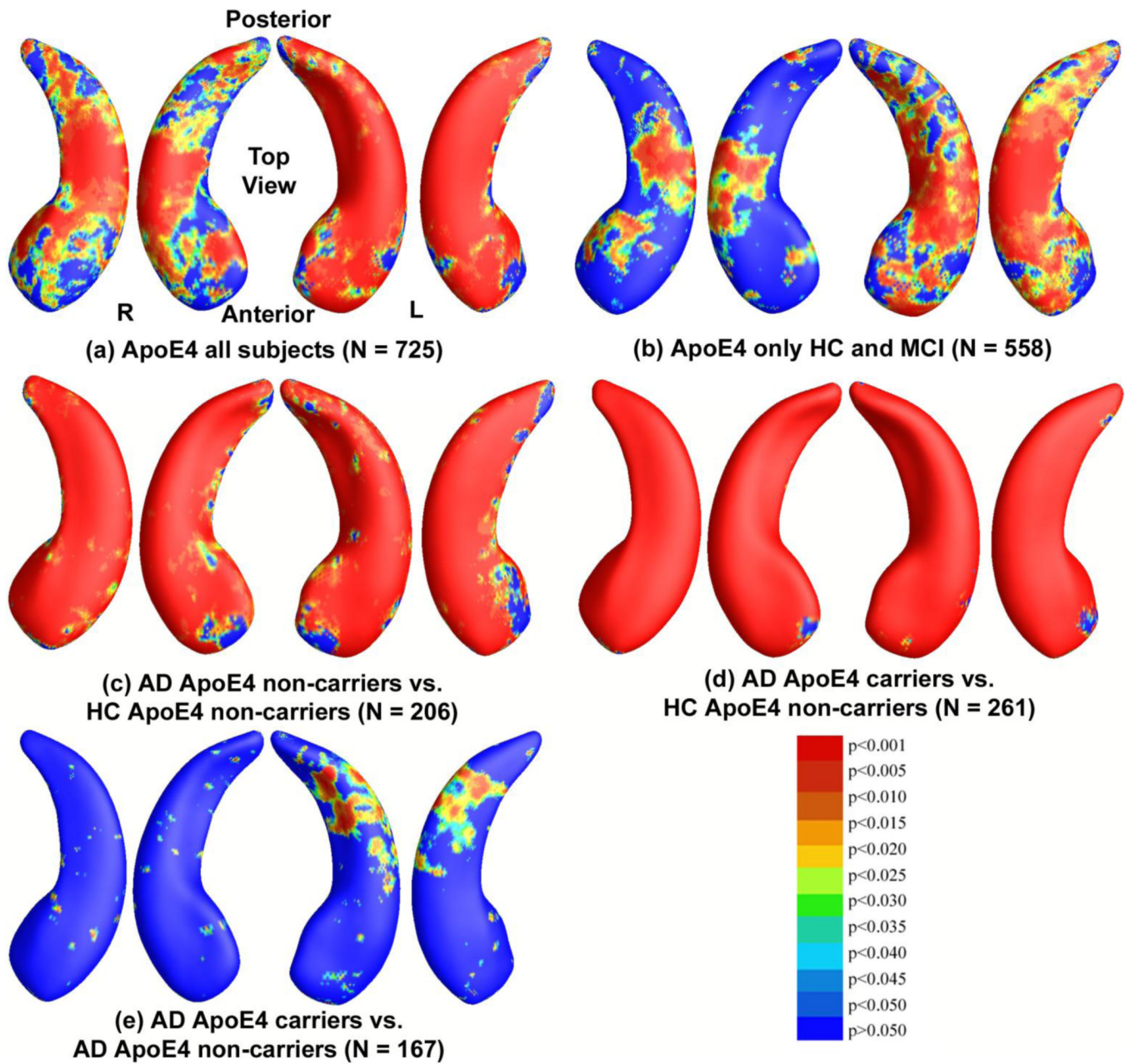


Figure 8. Significance maps for ApoE4 effects with inverse consistent surface fluid registration.

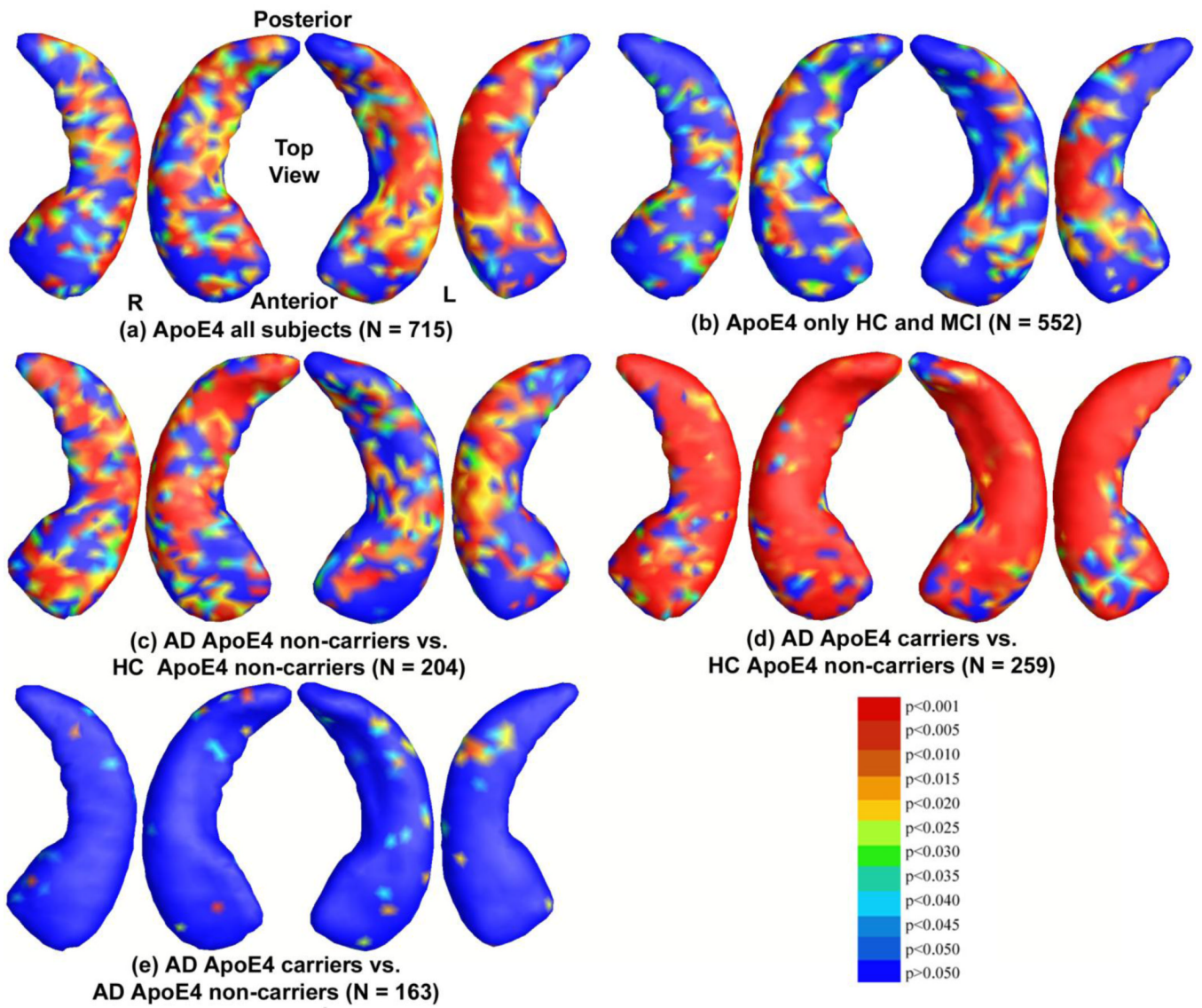


Figure 9. Significance maps for ApoE4 effects with FIRST method.

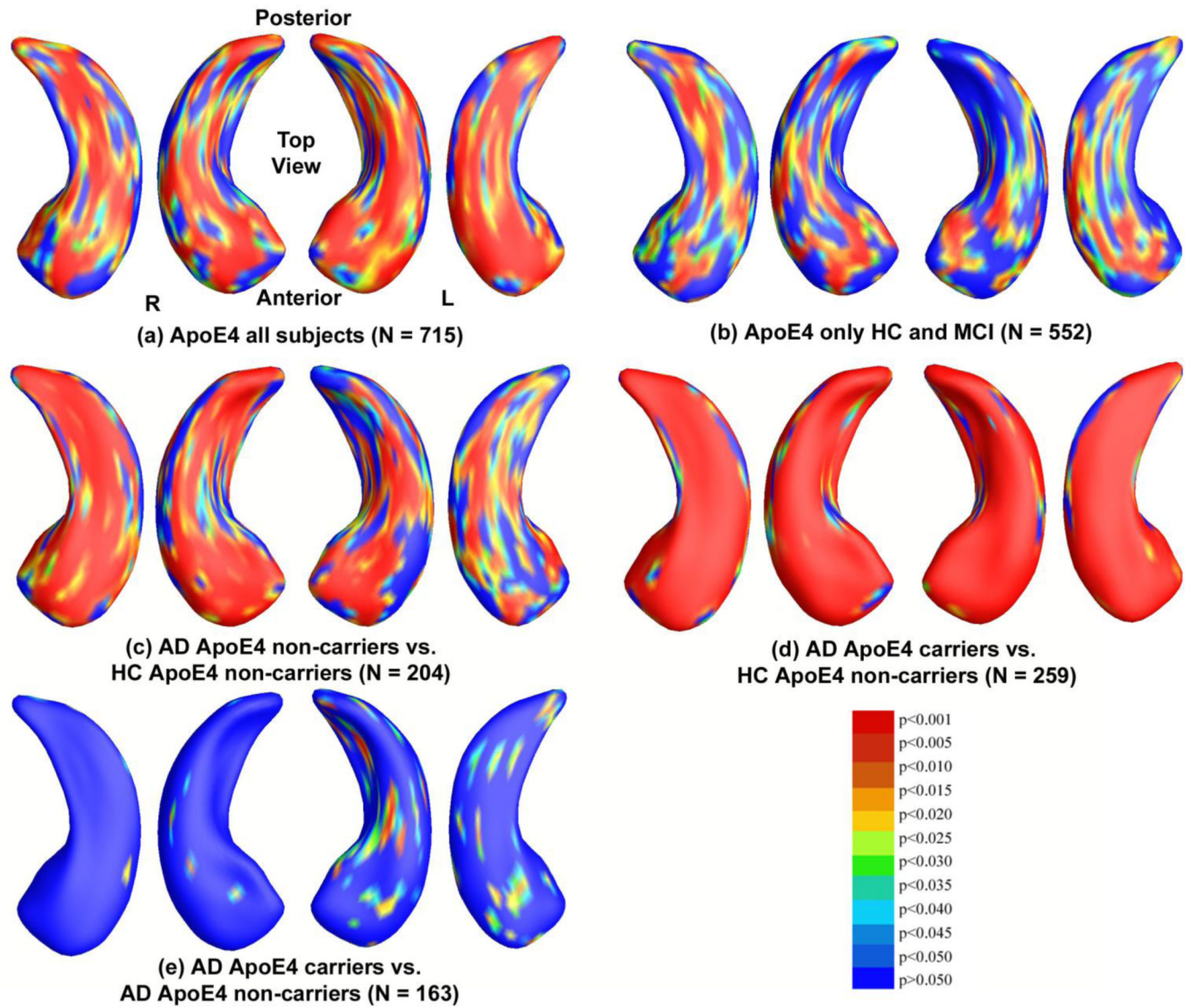
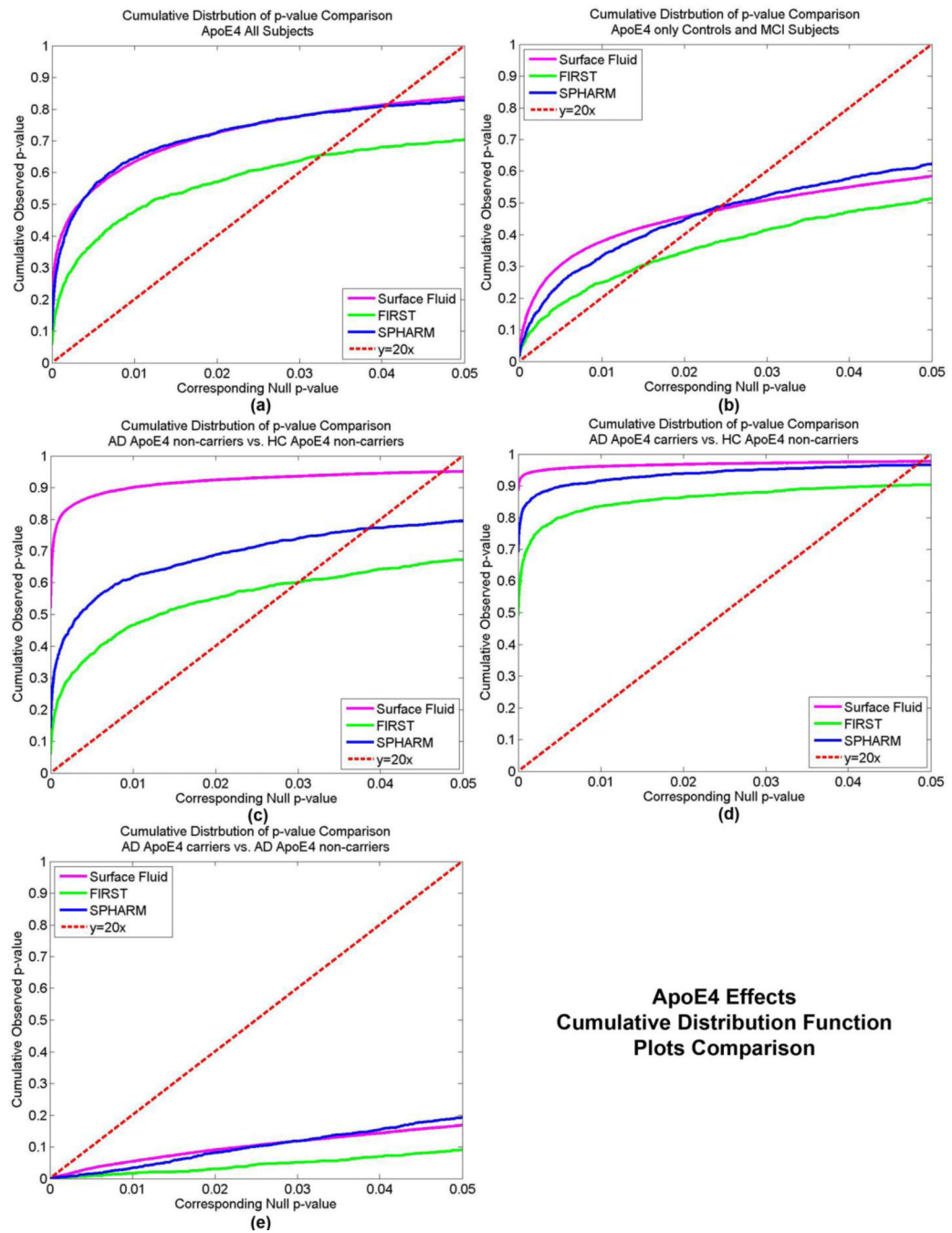


Figure 10.
Significance maps for ApoE4 effects with SPHARM method.



**ApoE4 Effects
Cumulative Distribution Function
Plots Comparison**

Figure 11. Cumulative distribution function plots comparison for ApoE4 effects with mTBM as the surface morphometry statistics.

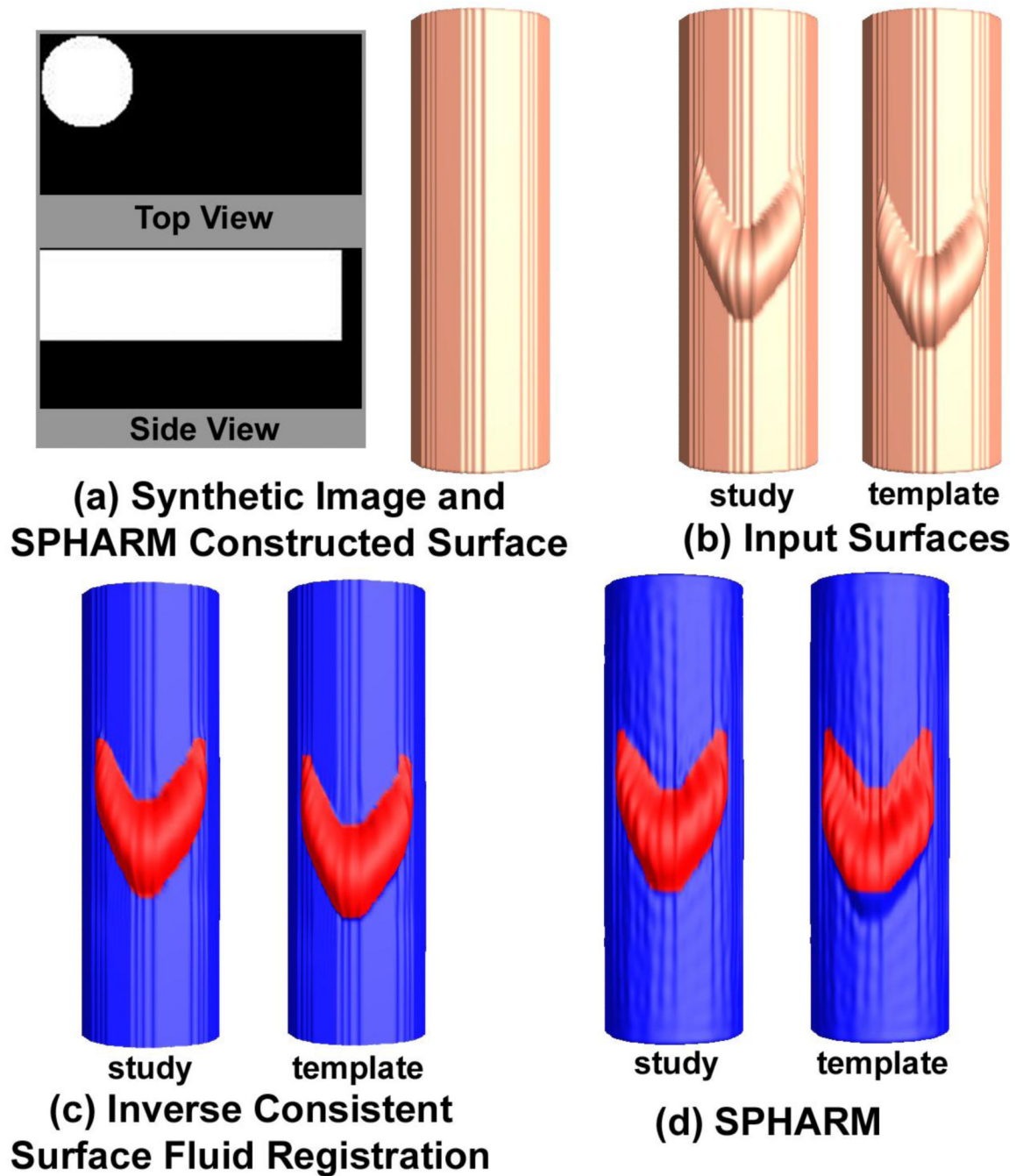


Figure 12.

Comparison of surface fluid registration and SPHARM on synthetic surfaces. (a) is the synthetic volumetric image for a cylinder and its surface model constructed with SPHARM tools. (b) shows the surfaces on which we put two synthetic C-shapes at different locations. (c) and (d) illustrate the surface registration achieved by inverse consistent surface fluid registration method (c) and SPHARM method (d). To show the registered correspondence, we drew the C-shape on the study surface with red color and transferred the color directly to the template surface. In (c) the C-shape on template surface is in red while in (d), the red color does not totally cover the C-shape. This simple experiment shows that our method register surface by matching detailed surface features.



Figure 13.

Comparison of the inverse consistent surface fluid registration with and without the area distortion correction term in Eq. 5. We visualize the pull-back metric by drawing those equal-spaced black strips defined on the target surfaces back to the source surfaces. Overall the registration results with the area distortion correction ((c) and (d)) are more uniform, i.e. less drastic area distortion strips, than the ones without the area distortion correction ((e) and (f)).

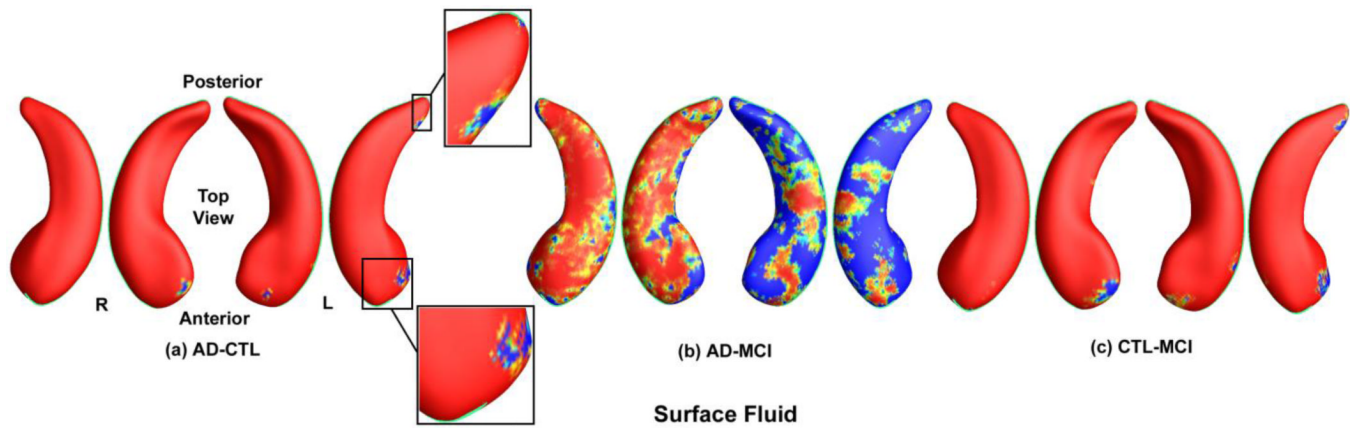


Figure 14. Positions of landmark curves and statistically insignificant regions on the p -maps of the inverse consistent surface fluid registration method. We can see that the statistically insignificant area does not align exactly with the cutting positions.

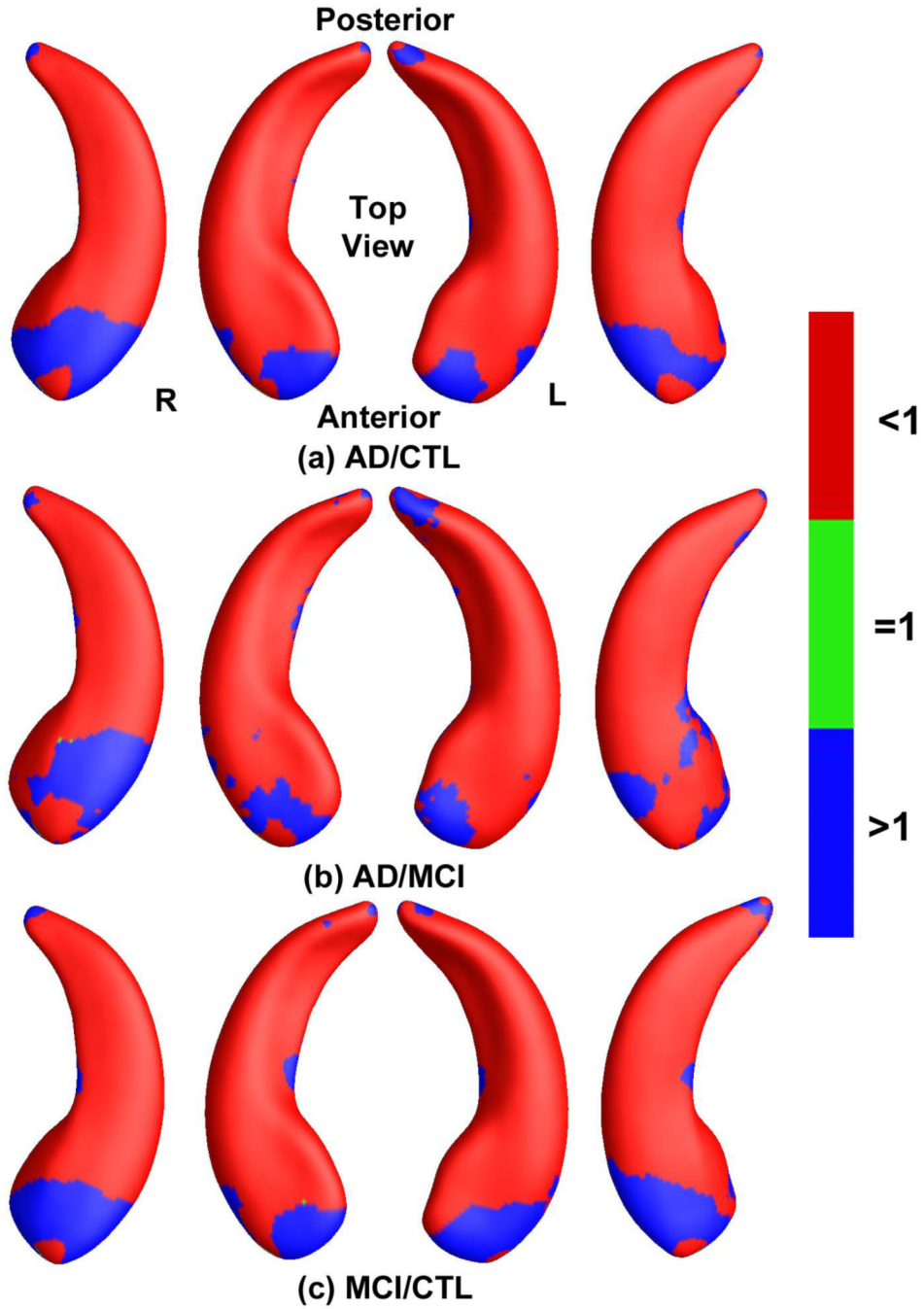


Figure 15. Maps of the ratios of average determinants of the Jacobian matrices R^k , defined in Eq. 12. (a) AD over control, (b) AD over MCI, (c) MCI over control. From the pictures, we can see the continuous increasing of the atrophy (red color) from control group to MCI and AD. There is also some enlargement areas (blue color). This is probably due to the tissue loss in the neighboring structures of hippocampus, which caused the shifting of the long axis of the hippocampus.

Table 1

FDR corrected p -values comparison. Our proposed system generated stronger statistical power than two other subcortical morphometry systems.

	Surface Fluid	FIRST	SPHARM
AD-CTL	0.0485	0.0455	0.0461
AD-MCI	0.0259	0.0058	0.0134
CTL-MCI	0.0479	0.0408	0.0468